

Updated Constraints on Omnipotent Dark Energy: A Comprehensive Analysis with CMB and BAO Data

Enrico Specogna,^{1,*} Shahnawaz A. Adil,^{2,†} Emre Özülker,^{1,‡} Eleonora Di Valentino,^{1,§} Rafael C. Nunes,^{3,4,¶} Özgür Akarsu,^{5,**} and Anjan A. Sen^{6,††}

¹*School of Mathematical and Physical Sciences, University of Sheffield, Hounsfield Road, Sheffield S3 7RH, United Kingdom*

²*Instituto de Ciencias Físicas, UNAM, Cuernavaca 62210, México*

³*Instituto de Física, Universidade Federal do Rio Grande do Sul, 91501-970 Porto Alegre RS, Brazil*

⁴*Divisão de Astrofísica, Instituto Nacional de Pesquisas Espaciais,*

Avenida dos Astronautas 1758, São José dos Campos, 12227-010, SP, Brazil

⁵*Department of Physics, Istanbul Technical University, Maslak 34469 Istanbul, Türkiye*

⁶*Centre for Theoretical Physics, Jamia Millia Islamia, New Delhi-110025, India.*

In this work, we present updated observational constraints on the parameter space of the DMS20 dark energy model, a member of the *omnipotent dark energy* (ODE) class. Our analysis combines multiple CMB datasets—including measurements from the Planck satellite (PL18), the South Pole Telescope (SPT), and the Wilkinson Microwave Anisotropy Probe (WMAP)—with Type Ia supernova data from the Pantheon+ catalog (PP), and baryon acoustic oscillation (BAO) measurements from the DESI and SDSS surveys. We find that certain data combinations, such as SPT+WMAP+BAO and PL18+BAO, can reduce the significance of the H_0 tension below 1σ , but with considerably large uncertainties. However, the inclusion of PP data restores the tension in H_0 . To provide a comprehensive view of the ODE phenomenology, we also investigate the evolution of its energy density, emphasizing its dynamical behavior at low redshifts. Our results generically exhibit multiple phantom divide line (PDL) crossings in a single expansion history, a behavior that is not compatible with single scalar field scenarios.

I. INTRODUCTION

The Λ CDM model has emerged as the dominant and most widely accepted cosmological framework. Its success is largely attributed to its remarkable accuracy in explaining a broad range of astrophysical and cosmological observations without excessive model complexity. Despite these successes, however, the Λ CDM model faces some unresolved challenges, particularly in capturing a consistent expansion history when various combinations of mainstream cosmological observables, such as the cosmic microwave background (CMB), baryon acoustic oscillations (BAO), large-scale structure (LSS), and local distance ladder measurements of the Hubble constant are simultaneously considered [1–5].

With the increasing precision of modern observations [6], it is anticipated that deviations from the standard Λ CDM model will become more apparent. Indeed, various discrepancies in the estimation of key cosmological parameters have already emerged, some of which show statistically significant departures from the predictions of the model [1, 2, 5, 7–10]. Among these issues, one of the most prominent and statistically significant is the ongoing discrepancy related to the Hubble constant, H_0 (for

a detailed review, see [1–3, 5, 9, 11–17] and references therein). A notable conflict exists between the values of H_0 inferred from the CMB measurements [18–20] assuming the Λ CDM model, and those derived from direct, independent measurements obtained through local astrophysical observations [21–47]. This tension, commonly referred to as the H_0 tension, has reached a statistical significance greater than 5σ [36, 37, 48], and is now considered one of the most pressing issues within the context of the Λ CDM model. To solve this tension, cosmologists have been exploring both possible systematic errors [29, 36, 38, 39, 48–57] and alternative cosmological models [1, 2, 5, 12, 14, 16, 58–63]. In addition to the H_0 tension, another point of discussion in cosmology is the S_8 tension [2, 7, 64, 65] (see also [66, 67]), which concerns discrepancies between the amplitude of matter fluctuations inferred from early-universe measurements, such as the Planck CMB data, and the S_8 values derived from late-time observations, including weak gravitational lensing and galaxy clustering, though it seems to have lost significance after the new KiDS-Legacy release [68–84]. Furthermore, recent results from the DESI collaboration analyzing the BAO feature have found evidence for dynamical dark energy (DDE) when their measurements are combined with other major observations [85–89]. This evidence for DDE is relevant only in the post-recombination era, with a statistical significance of 3.1σ when combined with the CMB. The significance ranges from 2.7σ to 4.2σ when different supernovae samples are included in the dataset combination. The indication persists even without the CMB; for example, only the DES supernovae sample [90] when combined with DESI BAO

* especogna1@sheffield.ac.uk

† shazadil14@gmail.com

‡ e.ozulker@sheffield.ac.uk

§ e.divalentino@sheffield.ac.uk

¶ rafadcnunes@gmail.com

** akarsuo@itu.edu.tr

†† aasen@jmi.ac.in

yields a 3.3σ significance. It is important to note that the evidence for DDE does not hinge on DESI BAO either, e.g., see Refs. [90, 91] that report preference of a DDE without this data set. A plethora of models have been proposed in the literature to address the existing cosmological tensions [5], a substantial portion of which incorporate a DDE component that is non-negligible in the late and/or early universe [85, 92–128].

The simplest phenomenological DDE model replaces the cosmological constant, whose effective equation of state (EoS) parameter is $w = -1$, with a DE fluid that has a constant EoS parameter able to satisfy $w_{\text{DE}} \neq -1$; this is often referred to as the w CDM model. Many models extend this approach by allowing a varying EoS parameter, with the most well-known example being the Chevallier-Polarski-Linder (CPL) parametrization [129, 130], in which w_{DE} is assumed to be a linear function of the scale factor in the Robertson–Walker (RW) metric. Notably, unless restricted to specific regions of parameter space, such extensions generically allow w_{DE} to cross the phantom divide line (PDL), $w_{\text{DE}} = -1$. However, parameterizing DDE solely via its EoS parameter fails to capture the phenomenology of models in which DDE attains negative effective energy densities in the past, as such components would exhibit a singular EoS parameter [131]. From both theoretical and phenomenological perspectives, models predicting negative energy densities in the dark sector have garnered increasing attention in recent years, particularly for their potential to resolve the H_0 tension [5, 86, 132–156]. DDE models capable of simultaneously incorporating all of these features were dubbed *omnipotent dark energy* (ODE) models in Ref. [157], where it was argued that such a flexible DDE component may be necessary for a satisfactory resolution of the prevailing cosmological tensions.

In Ref. [158], the DMS20 model was proposed as a promising solution to the cosmological tensions and was found to prefer a PDL crossing at $z \sim 0.1$. The recent analysis in Ref. [157] identified DMS20 as an ODE model and showed that its ability to reach negative energy densities for $z \gtrsim 2$ —mimicking a negative cosmological constant at high redshifts—plays a crucial role in alleviating the tensions. This behavior is consistent with the predictions of the Λ_s CDM model [138, 139, 143], which suggests a transition from an Anti-de Sitter (AdS) to a de Sitter (dS) phase. This transition can be interpreted either as an emergent effect from modified gravity or as the result of an actual field within the framework of general relativity (GR).

In this paper, we revisit and update the observational constraints on the DMS20 model using Type Ia supernova data from the Pantheon+ catalog, BAO measurements from the DESI and SDSS surveys, and CMB temperature and polarization data from Planck, the South Pole Telescope, and the Wilkinson Microwave Anisotropy Probe. Motivated by previous studies of the DMS20 model that reported posterior distributions leaning against the edges of the prior ranges for certain

dataset combinations, we extend these prior ranges. This not only relaxes the constraints on the model parameters but also enables the model to exhibit richer phenomenology that is qualitatively different—for example, a PDL crossing in the opposite direction. Nevertheless, we also present our results after excluding the MCMC samples corresponding to the extended priors, to facilitate direct comparison with previous studies.

The structure of this paper is organized as follows. In Section II, we review the key physical features of the omnipotent dark energy model, focusing on the aspects most relevant for cosmological tests. In Section III, we describe the observational datasets used in our analysis and outline the methodology employed to constrain the model’s free parameters. In Section IV, we present and discuss our main results, highlighting their implications for cosmological tensions and the broader landscape of dark energy models. Finally, in Section V, we summarize our conclusions and offer some perspectives on future research directions.

II. OMNIPOTENT DARK ENERGY: A REVIEW

In this section, we review the class of ODE models and the DMS20 model as a concrete member of this class. The term ODE describes a family of phenomenological proposals that allow energy densities to transition between positive and negative values, and to exhibit oscillatory or non-monotonic evolution histories. ODE models permit arbitrary EoS, including singularities and PDL crossings, unconstrained by standard energy conditions. As an effective source in the Friedmann equations, ODE provides a flexible framework to address the limitations of the cosmological constant. More precisely, a DE model is referred to as an ODE if, for any point in its parameter space, it can exhibit all six possible combinations of the conditions $\rho_{\text{DE}} > 0$, $\rho_{\text{DE}} < 0$, and $w_{\text{DE}} > -1$, $w_{\text{DE}} = -1$, $w_{\text{DE}} < -1$ within a single expansion history. Here, ρ_{DE} denotes the energy density of the DE component [157].

Two distinctive features of ODE are its capacity to realize a non-monotonic energy density evolution and to reach negative energy densities, as suggested by various observational reconstructions [153, 159–164]. Such behavior has been shown to alleviate key cosmological tensions, including the H_0 and S_8 discrepancies [132, 133, 135, 138, 139, 142, 158, 160, 165–169]. Hereafter, we consider an ODE component, whether as an effective source from modified gravity or a fluid within GR, that satisfies the usual continuity equation that follows from the local conservation of the energy-momentum tensor for the RW metric. Given this weak assumption, unlike usual phantom DE [170], which maintains $w_{\text{DE}} < -1$, the non-monotonicity feature of ODE models requires that its EoS parameter crosses the PDL. Moreover, since its energy density vanishes during the transition between negative and positive density regions at a scale factor a_p , its EoS parameter exhibits a pole of the

form $\lim_{a \rightarrow a_m^\pm} w_{\text{DE}}(a) = \mp\infty$; this also corresponds to a PDL crossing, but a discontinuous one [131].

The DMS20 model proposed in Ref. [158] serves as a concrete example of an ODE model. In this model, the DE density, ρ_{DE} , is parameterized to ensure an extremum at a scale factor a_m , satisfying the condition $\left. \frac{d\rho_{\text{DE}}}{da} \right|_{a=a_m} = 0$. The DE density is then expressed by expanding ρ_{DE} around a_m :

$$\rho_{\text{DE}}(a) = \rho_{\text{DE}0} \frac{1 + \alpha(a - a_m)^2 + \beta(a - a_m)^3}{1 + \alpha(1 - a_m)^2 + \beta(1 - a_m)^3}, \quad (1)$$

where α and β are constants defining the polynomial terms (for further details, see Refs. [157, 158]). The absence of a linear term in the expansion follows from the vanishing of the first derivative at $a = a_m$. The parameter a_m has significant physical implications: from the continuity equation, it follows that $w_{\text{DE}}(a_m) = -1$, provided that ρ_{DE} is non-zero at the extremum. For $\alpha > 0$, this corresponds to a transition from $w_{\text{DE}} > -1$ to $w_{\text{DE}} < -1$ as the universe expands, while for $\alpha < 0$, the crossing occurs in the opposite direction. The EoS for the ODE model is given by:

$$w_{\text{DE}}(a) = -1 - \frac{a[2\alpha(a - a_m) + 3\beta(a - a_m)^2]}{3[1 + \alpha(a - a_m)^2 + \beta(a - a_m)^3]}, \quad (2)$$

which yields $w_{\text{DE}}(a = 0) = -1$ and $w_{\text{DE}}(a \rightarrow \infty) = -2$.

This model introduces three extra parameters: $\{a_m, \alpha, \beta\}$. Depending on the values of these parameters, certain features of ODE may remain dormant. For instance, when $\alpha = \beta = 0$, the DE density reduces to the cosmological constant Λ , recovering the standard Λ CDM model. For a detailed discussion of the dynamical behavior of the model across different values of $\{a_m, \alpha, \beta\}$, see Ref. [157]. Here, we simply note that the EoS of DMS20 cannot be cast/remapped to the CPL parametrization, $w_{\text{DE}} = w_0 + w_a z / (1 + z)$, where $z = (1 - a) / a$ is the redshift. Here, $w_0 = w_{\text{DE}}(z = 0)$, and w_a is the first derivative of w_{DE} with respect to the scale factor. These two parameters are essential for characterizing the behavior of dark energy across a wide range of models, as discussed in [171], and both are constant parameters by construction in CPL. However, as shown in Fig. 1, for any choice of $\{a_m, \alpha, \beta\}$ we observe an oscillatory pattern in w_{DE} , which cannot be described by the linear CPL form. In fact, w_a would need to acquire a redshift dependence to account for the behavior of the EoS in Eq. (2). It is seen from Fig. 1 that variations in α significantly influence the present-day values of both w and w_a , while having a negligible effect at higher redshifts. Specifically, as α increases, w shifts further into the phantom regime, and w_a also increases. In the middle panel, we observe that β induces more pronounced oscillations in w , although its effect on w_a is relatively minor. Lastly, the parameter a_m shows a similar trend to α , highlighting its role in shaping the present-day dynamics of dark energy. It is evident that the linear CPL

parametrization fails to capture the non-linear features of the ODE model, whose oscillatory behavior cannot be reproduced by such a simplified form. With only one additional parameter, our ODE parametrization is thus able to recover a complementary class of DE models with a richer phenomenology.

To understand the background evolution of this model, we begin with the expansion rate of the universe, governed by the modified Friedmann equation:

$$\frac{H^2(a)}{H_0^2} = \Omega_{\text{m}0} a^{-3} + \Omega_{\text{r}0} a^{-4} + \Omega_{\text{DE}0} f(a), \quad (3)$$

where

$$f(a) = \frac{1 + \alpha(a - a_m)^2 + \beta(a - a_m)^3}{1 + \alpha(1 - a_m)^2 + \beta(1 - a_m)^3}. \quad (4)$$

In Eq. (3), the subscript “ m ” refers to all forms of matter (including both baryonic and cold dark matter), while “ r ” denotes radiation (photons and other relativistic relics). The density parameters $\Omega_{i0} \equiv \rho_{i0} / (3H_0^2)$ represent the present-day values of the respective energy densities.

The DMS20 model does not introduce modifications to other sectors of the universe or its constituent species. Consequently, the background evolution remains unchanged for all components other than DE itself. The linear evolution of DE perturbations follows the standard prescription, where we impose synchronous gauge conditions for metric perturbations. The continuity and Euler equations governing the DE fluid are given by

$$\begin{aligned} \dot{\delta}_x &= -(1 + w) \left(\theta + \frac{\dot{h}}{2} \right) - 3(\hat{c}_s^2 - w) \mathcal{H} \delta_x \\ &\quad - 9(1 + w)(\hat{c}_s^2 - c_a^2) \mathcal{H}^2 \frac{\theta_x}{k^2}, \end{aligned} \quad (5)$$

$$\dot{\theta}_x = -(1 - 3\hat{c}_s^2) \mathcal{H} \theta_x + \frac{\hat{c}_s^2 k^2}{1 + w} \delta_x - k^2 \sigma_x. \quad (6)$$

These equations are quite general, as they assume only a non-interacting fluid and allow for the presence of shear stress σ_x , a non-adiabatic sound speed, and a time-dependent equation of state parameter w . Henceforth, we assume the fluid is shear-free and that w is given by Eq. (2).

III. DATA AND METHODOLOGY

We generate theoretical predictions for the ODE model using a modified version of the Boltzmann solver CAMB [172, 173], while parameter estimation is performed with the publicly available sampler Cobaya [174]. The sampling of the posterior distributions is carried out using the Monte Carlo Markov Chain (MCMC) method, originally developed for CosmoMC [175]. This implementation incorporates the “fast dragging” technique [176, 177], which improves efficiency in exploring

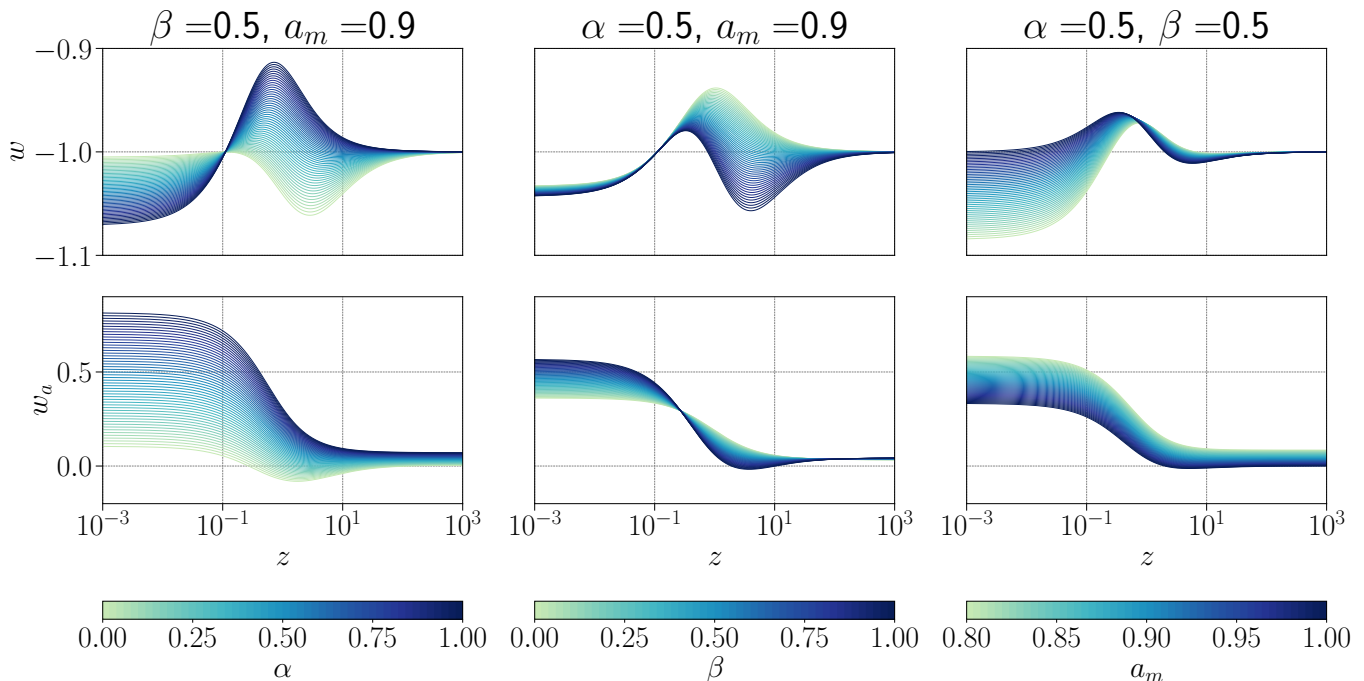


FIG. 1. The redshift evolution of w_{DE} and the CPL parameter w_a are shown for different values of $\{a_m, \alpha, \beta\}$. Clearly w_a cannot remain constant in this model, so the linear CPL parametrization of w_{DE} fails to capture the oscillatory behavior characteristic of ODE.

TABLE I. Flat priors are adopted to test the ODE model against all of the likelihood combinations presented in Sec. IV, with the exception of those involving the SPT+WMAP dataset combination, where a Gaussian prior is imposed on the optical depth: $\mathcal{P}(\tau) = \mathcal{N}(0.0544, 0.0073^2)$.

Parameter	Prior
$\Omega_b h^2$	[0.017, 0.027]
$\Omega_c h^2$	[0.09, 0.15]
τ	[0.01, 0.8]
n_s	[0.9, 1.1]
$\log(10^{10} A_s)$	[2.6, 3.5]
$100 \theta_{\text{MC}}$	[1.03, 1.05]
α	[-8, 8]
β	[-8, 8]
a_m	[0, 1.4]

parameter spaces with varying computational complexity.

In varying combinations, the likelihoods employed in this analysis use data from the following cosmological surveys:

- **Planck 2018 (PL18):** We include the full Planck 2018 temperature and polarization likelihoods (TT, TE, EE), along with the Planck 2018 lensing likelihood [18], reconstructed from the four-point correlation function of temperature fluctuations.

- **South Pole Telescope (SPT):** We incorporate CMB temperature and polarization anisotropy measurements (TT, TE, EE) from the SPT collaboration [19, 178].
- **Wilkinson Microwave Anisotropy Probe (WMAP):** We utilize CMB temperature and polarization data from the WMAP 9-year release [179]. To mitigate dust contamination, we exclude low- ℓ TE data and set the minimum multipole for TE at $\ell = 24$. When combining WMAP and SPT datasets, we consistently apply a Gaussian prior of $\tau = 0.0544 \pm 0.0073$.
- **Dark Energy Spectroscopic Instrument (DESI):** We include baryon acoustic oscillation (BAO) measurements from the DESI collaboration, based on galaxy and quasar observations [180], as well as Lyman- α tracers [181], compiled in Table I of Ref. [85]. These measurements span the redshift range $0.1 < z < 4.2$, divided into seven bins, and include both isotropic and anisotropic BAO constraints. The isotropic BAO measurements are expressed as $D_V(z)/r_d$, where D_V is the volume-averaged distance normalized to the comoving sound horizon at the drag epoch, r_d . The anisotropic constraints include $D_M(z)/r_d$ and $D_H(z)/r_d$, where D_M is the comoving angular diameter distance and D_H the Hubble horizon. Correlations between D_M/r_d and D_V/r_d are accounted for.

- **Sloan Digital Sky Survey (eBOSS):** We incorporate BAO data from the eBOSS experiment, including the DR16 measurements of D_M/r_d and D_H/r_d as obtained from luminous red galaxies and quasars as tracers only, and presented in Table 3 of Ref. [182].
- **Pantheon+ (PP):** We include distance modulus measurements of Type Ia supernovae from the Pantheon+ sample [183], consisting of 1,550 supernovae over the redshift range $0.001 \leq z \leq 2.26$.

For the DMS20 model parameters, we adopt the agnostic, flat priors outlined in Table I, except, as noted above, for an informative Gaussian prior on τ whenever the SPT+WMAP dataset combination is considered. Specifically, the parameter space of the DMS20 model extends the standard Λ CDM framework by introducing the three parameters defined in Eq. (1), namely α , β , and a_m , in addition to the six baseline Λ CDM parameters: the physical baryon and cold dark matter densities ($\Omega_b h^2$, $\Omega_c h^2$), the optical depth to reionization (τ), the amplitude and spectral index of the primordial scalar fluctuations ($\log(10^{10} A_s)$, n_s), and the angular size of the sound horizon at last scattering (θ_{MC}). Compared to Refs. [157, 158], the priors on α and β are extended to include negative values, and a_m is allowed to exceed 1, thereby enabling the possibility of PDL crossings occurring in the future (i.e., for $a > 1$). These choices are discussed in more detail in the next section.

All of the 1D and 2D posteriors were calculated and visualized using the `Getdist` code [184], while the functional posteriors for $w_{DE}(z)$ and $\rho_{DE}(z)$ shown in the next section were produced using the `fgivenx` plotting package [185].

IV. RESULTS AND DISCUSSION

We begin our discussion by justifying our choice of priors for the extra parameters of DMS20, namely, $\{a_m, \alpha, \beta\}$. In contrast to Refs. [157, 158], the prior ranges for $\{\alpha, \beta\}$ are chosen to include negative values, and the prior range for a_m is extended to include values greater than 1. In Refs. [157, 158], the choice of priors enforces $\alpha > 0$, $\beta > 0$, and $a_m \in [0, 1]$. This restricts ρ_{DE} to an evolution history with certain properties, the most important being the guaranteed existence of a PDL crossing at $a = a_m$, where the EoS parameter transitions from $w_{DE} > -1$ to $w_{DE} < -1$ as the universe expands. However, in both of the previous studies, the reported posteriors for these parameters do not exclude the prior bounds for many of the dataset combinations, particularly those that do not include the SH0ES H_0 measurement. Moreover, recent indications of a dynamical dark energy component suggest evidence for a preference of a

PDL crossing in the opposite direction,¹ i.e., where the EoS parameter transitions from $w_{DE} < -1$ to $w_{DE} > -1$ as the universe expands [85, 88]. In fact, the PDL crossing at $a = a_m$ occurs in this opposite direction when $\alpha < 0$. More generally, various qualitatively different DE density evolution histories become available in the DMS20 model when the parameters are allowed to explore this extended parameter space; see Table II and Fig. 1 of Ref. [157] and the discussions therein.

In this work, we chose the extended priors in Table I to take a more conservative approach that does not guarantee the existence of a_m within the expansion history, and allowed the MCMC analysis to explore the parameter space of the model more freely. Indeed, the results we report suggest that these extended regions of parameter space are always consistent with our dataset combinations, and are sometimes even preferred. To better compare our results with previous works, we also report results obtained after filtering the MCMC chains by dropping any samples with $\alpha < 0$, $\beta < 0$, or $a_m > 1$. We ensured that all of the filtered chains satisfied the Gelman–Rubin convergence criterion with $R - 1 < 0.09$; this approach is equivalent to performing the analysis with the corresponding restricted priors. We refer to the results from the full chain as the “full-prior results,” and to those from the post-processed chains as the “post-filtered results.”

In this section, we present the main results of our analysis using different combinations of datasets. We analyze constraints on our dynamical dark energy model ODE, characterized by the parameters α , β , and a_m , using various combinations of the CMB and BAO measurements described in the previous section, with and without supernovae distance moduli.

In Figs. 2 and 3, we present the parameter constraints derived from both the full-prior and post-filtered analyses. We find that using the full priors results in multimodal posterior distributions for certain parameters, while the post-filtered analysis yields unimodal distributions. The multimodality in the full results arise from the phenomenological degeneracies in the parameter space, i.e., different regions of the parameter space correspond to similar expansion histories; see Tab. II in [157]. The Λ CDM model is nested in DMS20 and correspond to the $\alpha = \beta = 0$ section of the parameter space. It is seen from Fig. 3 that this section corresponding to Λ CDM is perfectly consistent with all of the data set combinations shown on the triangular plot and there is no evidence for dynamics in the DE density evolution.

¹ It is important to note that the prior ranges chosen in Refs. [157, 158] allow (but do not guarantee) for a second PDL crossing in this opposite direction in addition to the one at $a = a_m$, and even a third crossing may occur in a discontinuous way if the DE density attains negative values in the past. In fact, when the model is constrained with data, all three of these crossings were found to play an important role in the evolution of the DE density.

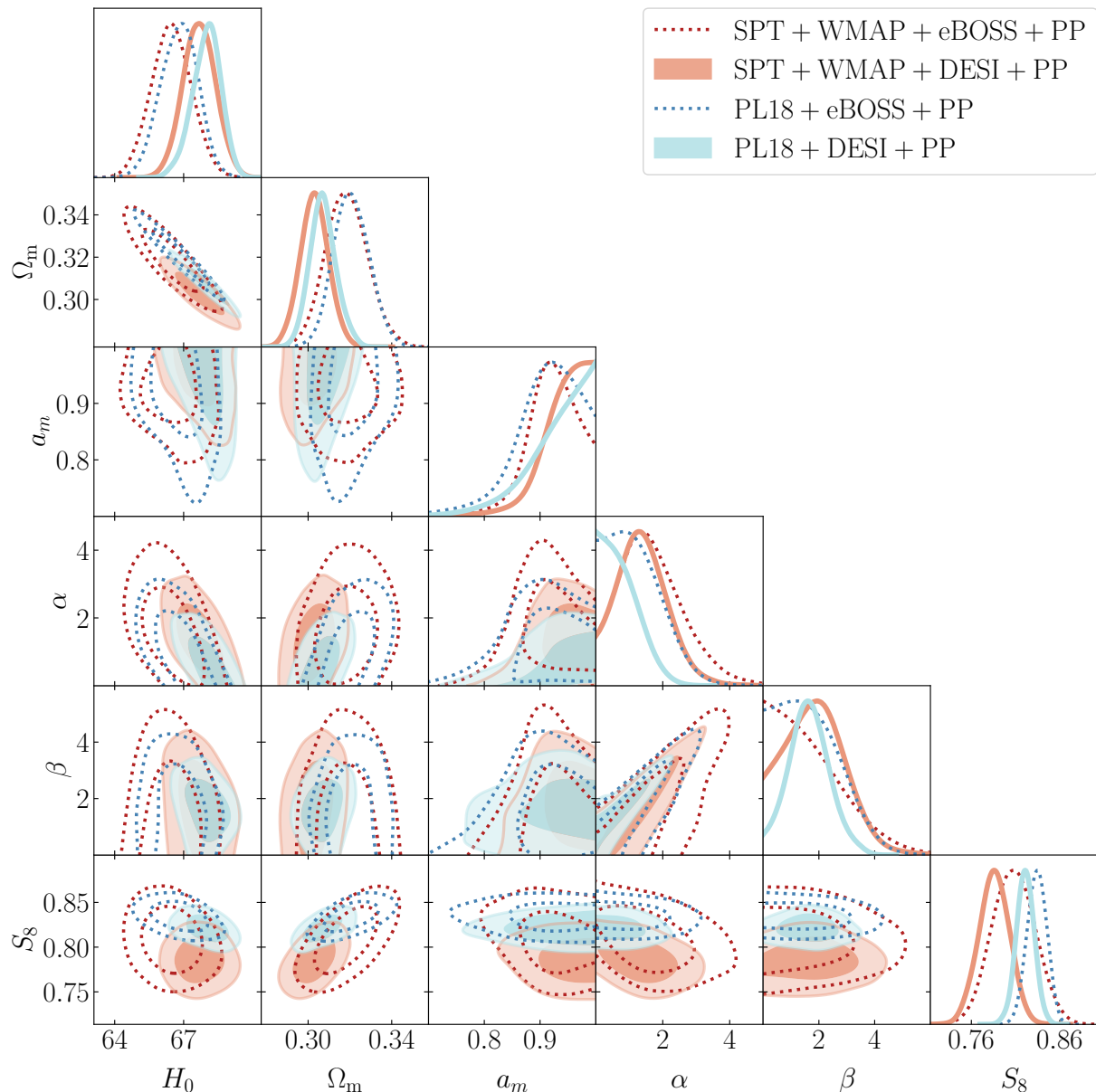


FIG. 2. 1D and 2D marginalized constraints on the ODE parameter space, derived from the post-filtered chains that include only samples with $\alpha > 0$, $\beta > 0$, and $a_m \in [0, 1]$.

Overall, despite the different prior choices (to be discussed in detail later), the results remain statistically consistent across all analyses. A comparative analysis of the SPT+WMAP+DESI+PP and PL18+DESI+PP combinations shows that the latter yields tighter parameter constraints, as illustrated by the red and blue contour plots. Moreover, the inferred value of S_8 is systematically lower when using the SPT+WMAP+DESI+PP combination compared to PL18+DESI+PP. Substituting DESI with eBOSS leads to additional shifts in the best-fit values of several parameters, highlighting the sensitivity of the results to the choice of BAO dataset. We note that our eBOSS compilation is considerably different than the BAO data in

both of the Refs. [157, 158]; this is the main factor that drives the differences in our results in comparison.

We present the complete set of parameter estimates from our analysis in Tables II–V. Post-filtered results show significantly tighter constraints on cosmological parameters compared to the full-prior setup. In both the SPT and PL18 cases, the parameters α , β , and a_m are more precisely determined when the prior ranges on model parameters are restricted. This is expected as the post-filtering removes a significant portion that is within 68% CL of the mean values of the marginalized posteriors. The inclusion of PP data further enhances the precision of these constraints. For instance, the

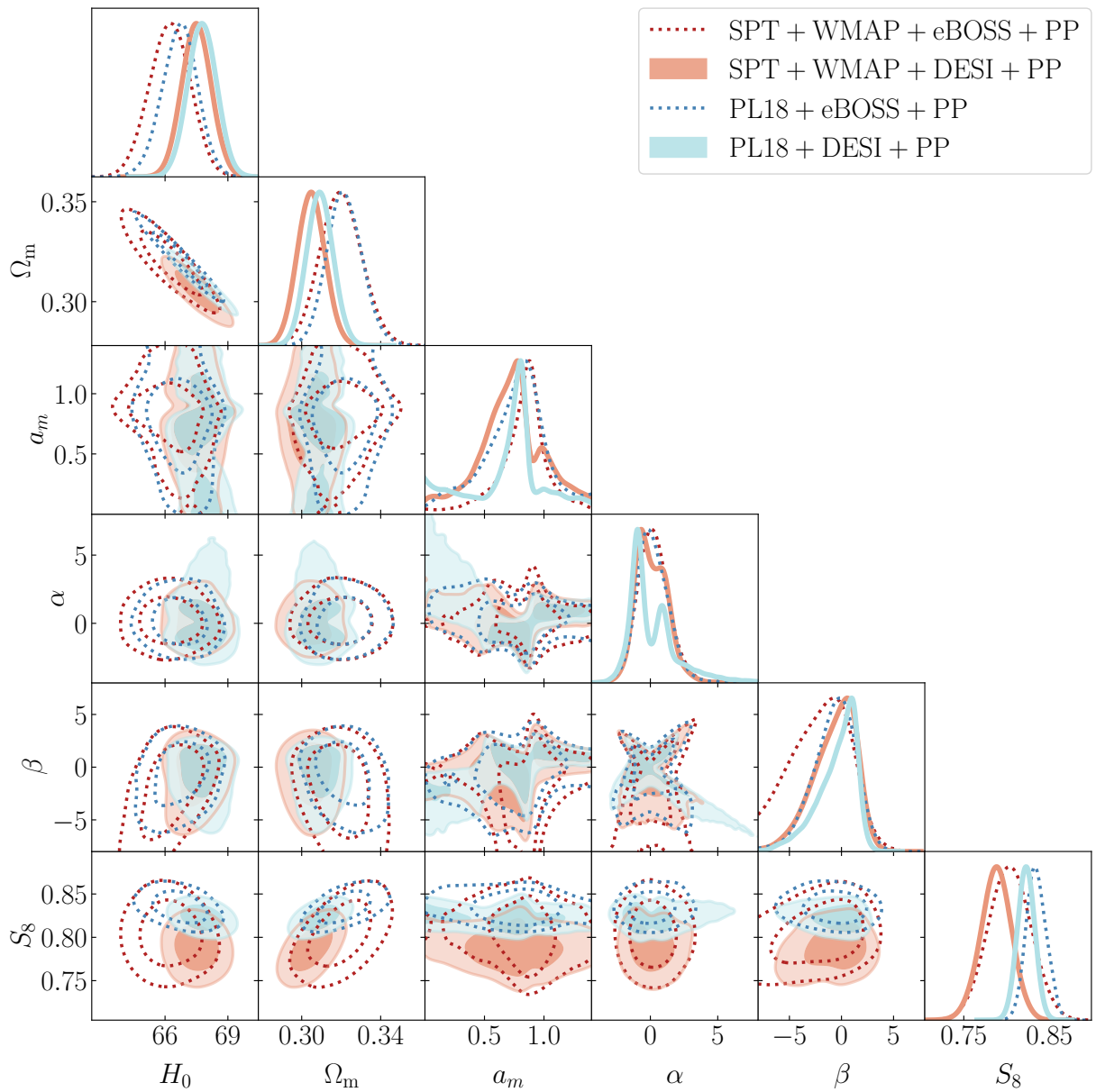


FIG. 3. 1D and 2D marginalized constraints on the ODE parameter space, obtained from the chains sampled with the full prior ranges listed in Table I, without any post-processing cuts (full-prior results).

SPT+WMAP+DESI+PP combination with post-filtered priors (see Table II) yields, at 68% CL, $\alpha = 1.40^{+0.65}_{-0.84}$, $\beta = 1.88^{+0.95}_{-1.2}$, and $a_m > 0.930$. In contrast, the same dataset under the full-prior setup gives $\alpha = 0.1^{+1.0}_{-1.3}$, $\beta = -0.7^{+2.5}_{-1.5}$, and $a_m = 0.73 \pm 0.28$ at 68% CL (see Table III).

While the full-prior results are better for interpreting the true phenomena that our data sets prefer, the post-filtered results are easier to interpret and match the previous studies [157, 158]. The post-filtered results enforce the existence of a DE EoS parameter that crosses from a quintessence regime to phantom regime at $a = a_m$. For instance, we see in Table IV that PL18+eBOSS

yields a clear peak for the scale of the PDL crossing at $a_m = 0.72^{+0.22}_{-0.11}$ and the addition of PP significantly reduces the uncertainties and yields $a_m = 0.907^{+0.078}_{-0.030}$. This is accompanied by a reduction in the uncertainty of H_0 that goes from $H_0 = 71.0^{+3.6}_{-6.0}$ that is consistent with the SH0ES measurement to $H_0 = 66.80 \pm 0.81$ that is not better than the Planck Λ CDM. Interestingly, replacing the eBOSS data with the newer DESI dataset further tightens the constraints on the ODE parameters α , β , and H_0 . The Hubble constant shifts slightly toward higher values, reflecting the preference of DESI for a lower matter density relative to eBOSS, and the well-known anti-correlation between H_0 and Ω_m . However,

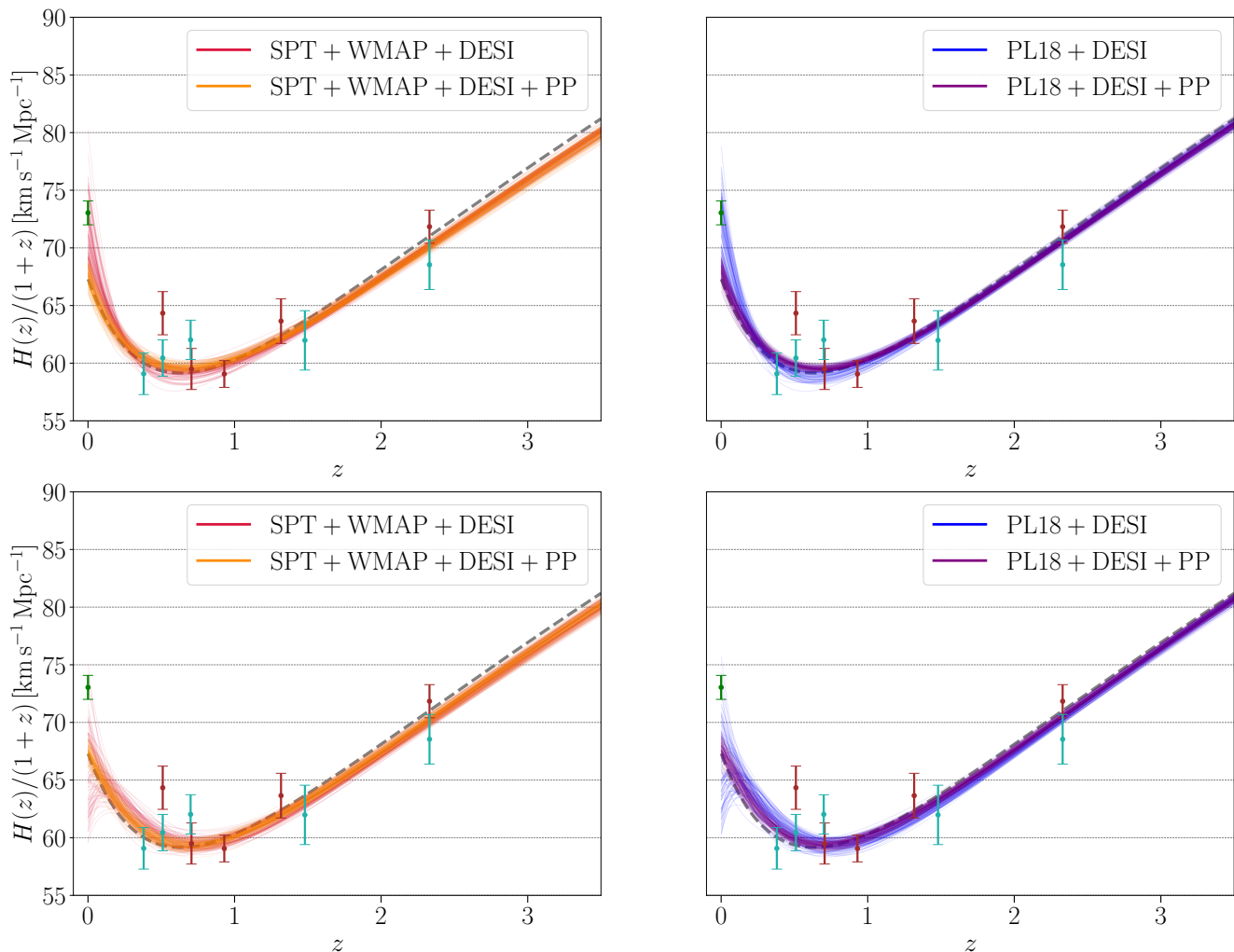


FIG. 4. ODE constraints (top panels post-filtered results, bottom panels full prior results) on the redshift evolution of the $H(z)/(1+z)$ function, derived from the SPT+WMAP+DESI and PL18+DESI data combinations, with and without supernovae. Also shown are D_H/r_d measurements from eBOSS [186] (green) and DESI YR1 [85] (red), obtained using luminous red galaxies, emission line galaxies, and quasars as tracers; the point at $z=0$ is the SH0ES constraint $H_0 = 73.04 \pm 1.04 \text{ km s}^{-1} \text{ Mpc}^{-1}$ [48]. These measurements are converted into $H(z)$ using the Planck constraint $r_d = 147.09 \pm 0.26 \text{ Mpc}$. The grey dashed line represents the ΛCDM best-fit curve from TTTEEE+lowE+lensing [18].

for the complete set PL18+DESI+PP, the clear peak for a_m disappears and we only have a lower bound; this implies that this data combination do not prefer a PDL crossing of this type in line with the findings of Refs. [85, 91] that find a preference for a PDL crossing in the opposite direction at late times when CMB data is combined with DESI+PP. We remind that a PDL crossing in this opposite direction occur also in our post-filtered results, the difference is that it is followed by the second PDL crossing at $a = a_m$; see Figs. 5 and 7.

When we replace PL18 with SPT as the baseline (see Table II), we see that the comparisons between BAO data sets and the effect of addition of PP are qualitatively the same; however, the values of the parameters change considerably between these different CMB data sets. We observe that for the SPT+WMAP+eBOSS combina-

tion, the mean value of H_0 is noticeably lower compared to the corresponding result with PL18. In this case too, however, replacing eBOSS with DESI leads to a significant shift of the Hubble constant towards higher values, with $H_0 = 71.0^{+1.8}_{-3.2} \text{ km/s/Mpc}$, in agreement with local measurements within 1σ , along with a correspondingly lower matter density. Moreover, as in the results with PL18, the addition of PP shifts all parameters back toward ΛCDM -like values.

Different behaviors are observed when analyzing the model with the full priors. As shown in Tables III and V, β consistently prefers a mean value in the negative region, with the 68% CL for the SPT+WMAP+DESI case being negative, and the PL18+DESI case having an upper bound of -2.12 . Hence, we see that the post-filtering forces the β values to be larger. One could expect, in parallel, that

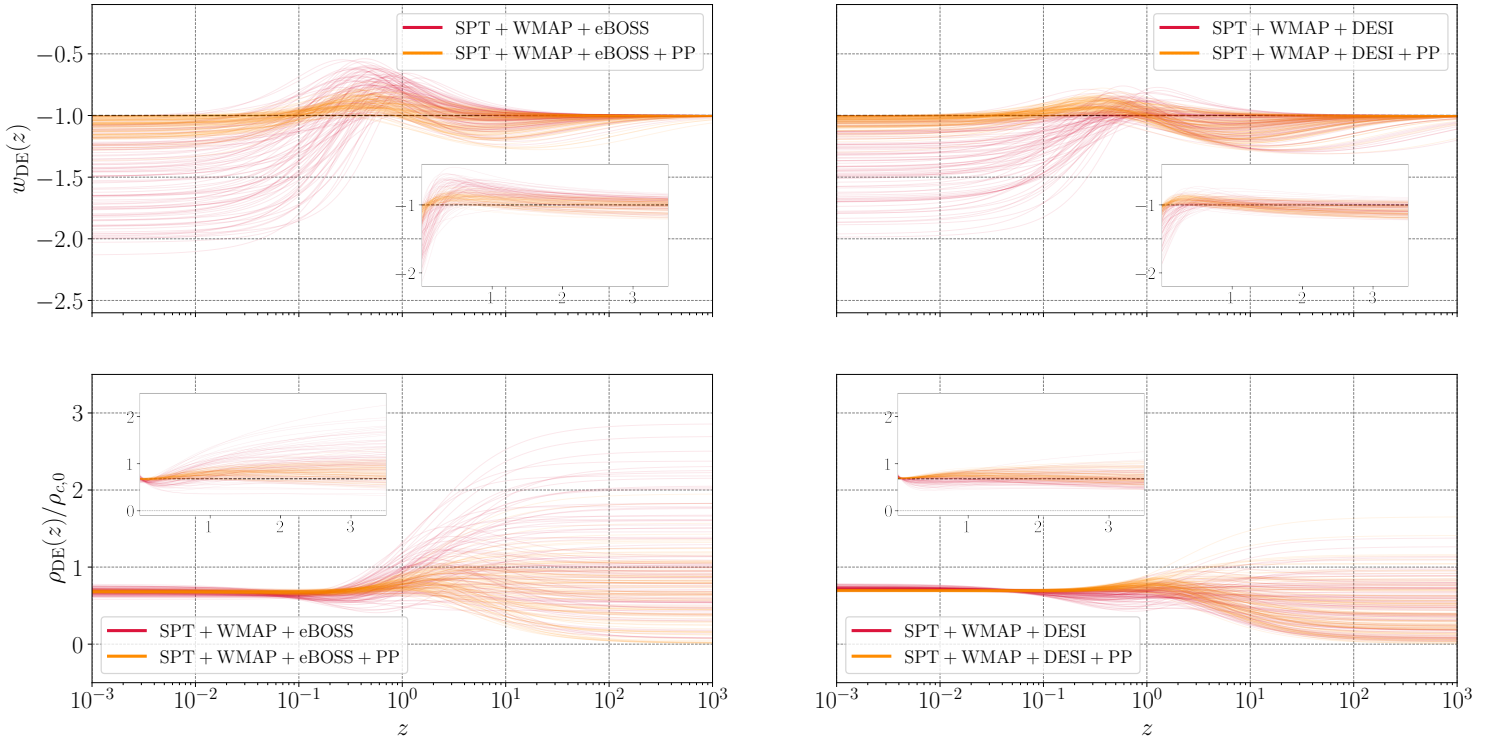


FIG. 5. Redshift evolution of $w_{\text{DE}}(z)$ (top panels) and $\rho_{\text{DE}}(z)/\rho_{c,0}$ (bottom panels) obtained from the post-filtered results using SPT as the baseline CMB dataset. In each panel the reader can find the same plot contained in the panel itself, re-expressed through a linear but shorter redshift range.

TABLE II. 68% CL constraints on the free parameters (above the line) and derived parameters (below the line), obtained from the post-filtered results using SPT as the baseline CMB dataset.

	SPT+WMAP +eBOSS	SPT+WMAP +eBOSS+PP	SPT+WMAP +DESI	SPT+WMAP +DESI+PP
$\Omega_b h^2$	0.02240 ± 0.00020	0.02238 ± 0.00020	0.02244 ± 0.00020	0.02244 ± 0.00019
$\Omega_c h^2$	0.1168 ± 0.0023	0.1176 ± 0.0022	$0.1157^{+0.0016}_{-0.0014}$	0.1157 ± 0.0016
$100\theta_{MC}$	1.04016 ± 0.00066	1.04010 ± 0.00066	1.04028 ± 0.00062	1.04029 ± 0.00064
τ	0.0532 ± 0.0072	0.0530 ± 0.0071	0.0538 ± 0.0070	0.0537 ± 0.0070
$\ln(10^{10} A_s)$	3.032 ± 0.015	3.034 ± 0.015	3.030 ± 0.015	3.030 ± 0.015
n_s	0.9674 ± 0.0062	0.9660 ± 0.0061	0.9690 ± 0.0055	0.9691 ± 0.0055
α	$4.1^{+2.5}_{-2.0}$	$1.68^{+0.71}_{-1.1}$	< 1.80	$1.40^{+0.65}_{-0.84}$
β	< 4.91	< 2.16	< 2.98	$1.88^{+0.95}_{-1.2}$
a_m	> 0.786	$0.918^{+0.053}_{-0.035}$	$0.74^{+0.16}_{-0.12}$	> 0.930
Ω_m	$0.307^{+0.043}_{-0.038}$	0.318 ± 0.010	$0.276^{+0.025}_{-0.016}$	0.3030 ± 0.0069
H_0 [km/s/Mpc]	$67.9^{+3.2}_{-5.5}$	66.47 ± 0.87	$71.0^{+1.8}_{-3.2}$	67.68 ± 0.71
S_8	0.793 ± 0.028	0.808 ± 0.024	$0.775^{+0.020}_{-0.017}$	0.786 ± 0.018
r_{drag} [Mpc]	147.92 ± 0.59	147.74 ± 0.58	148.16 ± 0.44	148.18 ± 0.45
$\Delta\chi^2_{\text{min}}$	-0.67	1.5	1.8	-1.4

post-filtering would shift the a_m constraints to lower values by dropping the $a_m > 1$ samples in the chain. However, in contrast, the favored values of a_m are smaller for the full-prior, resulting in only an upper limit when DESI data are used with Planck. This is due to the correlations

between $\{\alpha, \beta, a_m\}$. Finally, although α appears to have significantly larger uncertainties, Fig. 3 shows that its posterior is bimodal around zero for the DESI data, with the peak for the negative values corresponding to a larger probability.

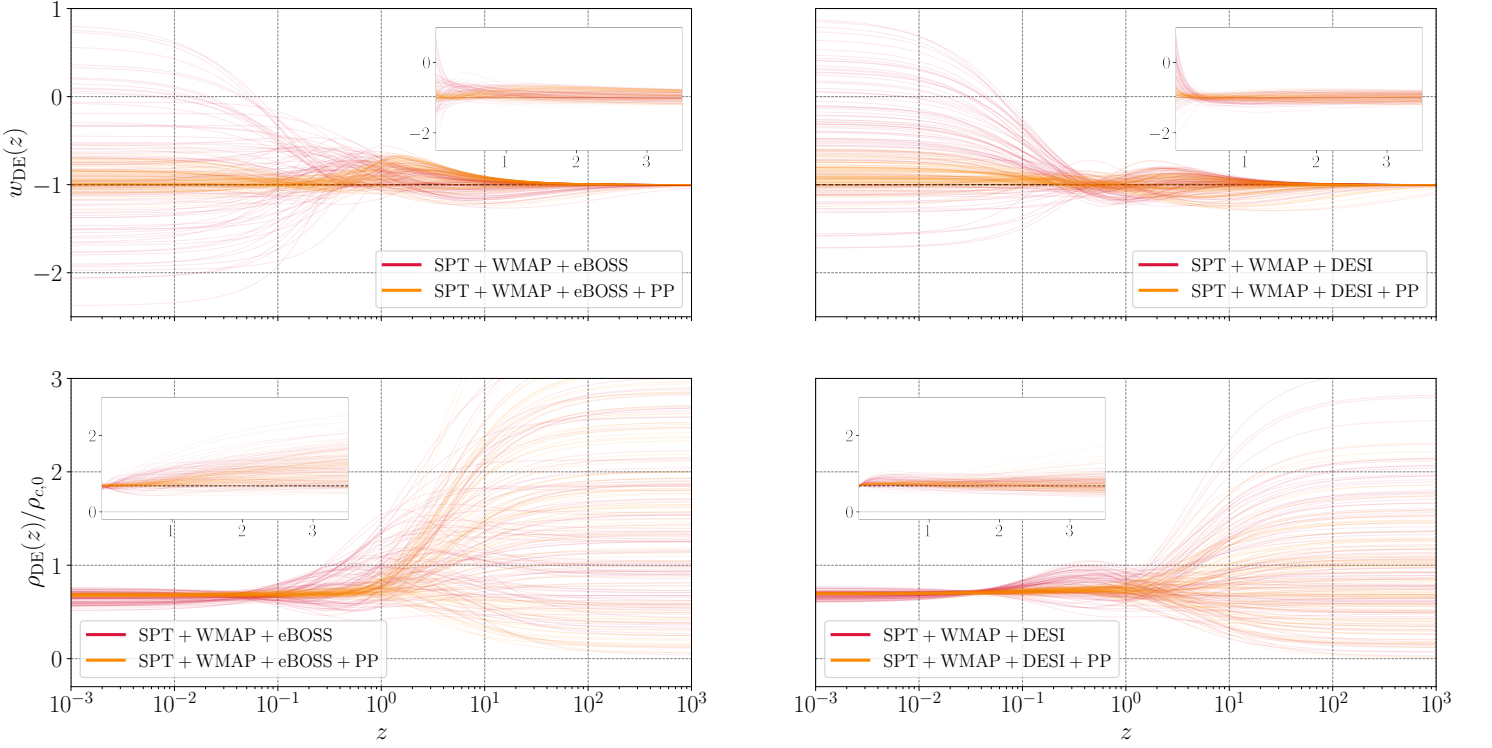


FIG. 6. Same as Fig. 5 but for the full-prior results.

TABLE III. 68% CL constraints on the free parameters (above the line) and derived parameters (below the line), obtained from the full-prior results using SPT as the baseline CMB dataset.

	SPT+WMAP +eBOSS	SPT+WMAP +eBOSS+PP	SPT+WMAP +DESI	SPT+WMAP +DESI+PP
$\Omega_b h^2$	0.02240 ± 0.00020	0.02239 ± 0.00021	0.02243 ± 0.00020	0.02244 ± 0.00020
$\Omega_c h^2$	0.1169 ± 0.0023	0.1172 ± 0.0022	0.1159 ± 0.0017	0.1158 ± 0.0016
$100\theta_{MC}$	1.04015 ± 0.00066	1.04013 ± 0.00066	1.04026 ± 0.00064	1.04029 ± 0.00064
τ	0.0531 ± 0.0072	0.0531 ± 0.0072	0.0535 ± 0.0072	0.0536 ± 0.0072
$\ln(10^{10} A_s)$	3.032 ± 0.016	3.033 ± 0.015	3.030 ± 0.015	3.030 ± 0.015
n_s	0.9672 ± 0.0063	0.9666 ± 0.0061	0.9686 ± 0.0056	0.9689 ± 0.0055
α	2.0 ± 3.2	$0.2^{+1.1}_{-1.2}$	$0.6^{+2.3}_{-3.1}$	$0.1^{+1.0}_{-1.3}$
β	$0.4^{+5.0}_{-3.3}$	$-2.0^{+3.2}_{-2.5}$	$-2.6^{+2.3}_{-4.6}$	$-0.7^{+2.5}_{-1.5}$
a_m	$0.81^{+0.47}_{-0.23}$	$0.82^{+0.20}_{-0.16}$	0.58 ± 0.28	0.73 ± 0.28
Ω_m	0.344 ± 0.051	0.320 ± 0.011	$0.323^{+0.036}_{-0.041}$	0.3048 ± 0.0071
H_0 [km/s/Mpc]	$64.3^{+3.5}_{-5.9}$	66.23 ± 0.97	$65.9^{+3.6}_{-4.2}$	67.50 ± 0.70
S_8	0.807 ± 0.031	0.803 ± 0.025	0.796 ± 0.024	0.788 ± 0.018
r_d [Mpc]	147.89 ± 0.60	147.83 ± 0.59	148.12 ± 0.47	148.16 ± 0.46
$\Delta\chi^2_{min}$	-0.67	0.30	-2.4	-3.4

In our analysis, the inferred values of the Hubble constant H_0 remain consistently lower than the SH0ES measurement ($H_0 = 73.04 \pm 1.04$ km/s/Mpc), though the extent of the discrepancy varies across datasets. For example, the SPT+WMAP+eBOSS combination yields $H_0 = 67.9^{+3.2}_{-5.5}$ km/s/Mpc with post-filtered priors (Table II),

and $H_0 = 64.3^{+3.5}_{-5.9}$ km/s/Mpc with full priors (Table III). In contrast, the PL18+DESI+PP combination provides a more precise full prior estimate of $H_0 = 67.77 \pm 0.69$ km/s/Mpc (Table V). Although certain configurations formally yield a significantly reduced tension with the SH0ES measurement (e.g., for the analyses without PP),

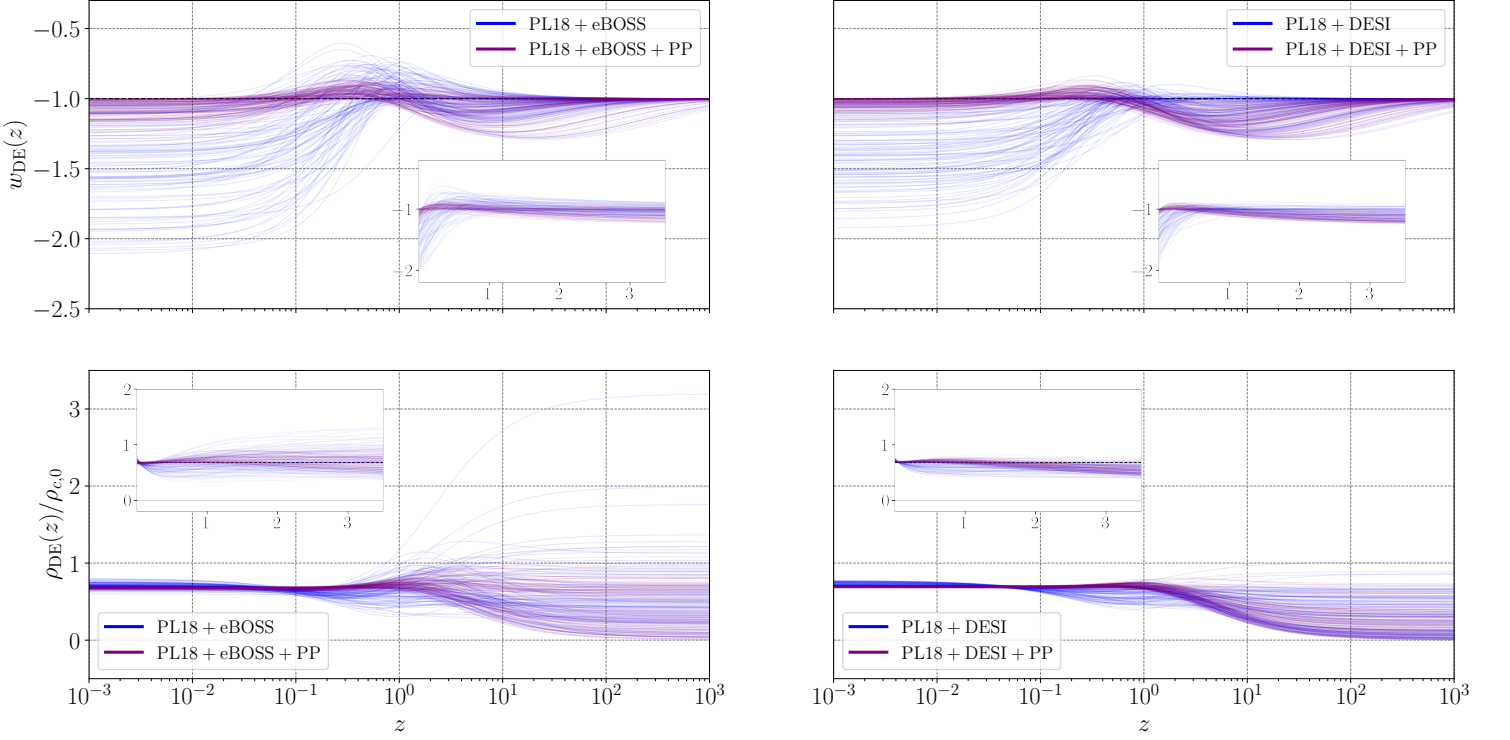


FIG. 7. Redshift evolution of $w_{\text{DE}}(z)$ (top panels) and $\rho_{\text{DE}}(z)/\rho_{c,0}$ (bottom panels) obtained from the post-filtered results using PL18 as the baseline CMB dataset. In each panel the reader can find the same plot contained in the panel itself, re-expressed through a linear but shorter redshift range.

TABLE IV. 68% CL constraints on the free parameters (above the line) and derived parameters (below the line), obtained from the post-filtered results using PL18 as the baseline CMB dataset.

	PL18+eBOSS	PL18+eBOSS+PP	PL18+DESI	PL18+DESI+PP
$\Omega_b h^2$	0.02238 ± 0.00014	0.02237 ± 0.00014	0.02248 ± 0.00014	0.02247 ± 0.00014
$\Omega_c h^2$	0.1200 ± 0.0011	0.1200 ± 0.0011	0.11860 ± 0.00093	0.11883 ± 0.00098
$100\theta_{MC}$	1.04092 ± 0.00029	1.04091 ± 0.00031	1.04113 ± 0.00028	$1.04107^{+0.00030}_{-0.00026}$
τ	0.0546 ± 0.0073	0.0546 ± 0.0076	0.0574 ± 0.0076	0.0571 ± 0.0077
$\ln(10^{10} A_s)$	3.045 ± 0.014	3.045 ± 0.015	3.048 ± 0.015	3.048 ± 0.015
n_s	0.9654 ± 0.0040	0.9654 ± 0.0040	0.9688 ± 0.0038	0.9683 ± 0.0038
α	< 3.20	< 1.51	< 1.02	< 1.01
β	< 4.48	< 2.19	< 2.84	1.66 ± 0.72
a_m	$0.72^{+0.22}_{-0.11}$	$0.907^{+0.078}_{-0.030}$	$0.66^{+0.26}_{-0.13}$	> 0.913
Ω_m	$0.288^{+0.042}_{-0.038}$	0.3207 ± 0.0085	$0.277^{+0.030}_{-0.019}$	$0.3071^{+0.0058}_{-0.0067}$
H_0 [km/s/Mpc]	$71.0^{+3.6}_{-6.0}$	66.80 ± 0.81	$71.7^{+2.3}_{-3.9}$	$67.99^{+0.68}_{-0.56}$
S_8	$0.818^{+0.022}_{-0.018}$	0.834 ± 0.011	$0.806^{+0.015}_{-0.013}$	0.821 ± 0.010
r_{drag} [Mpc]	147.10 ± 0.25	147.09 ± 0.26	147.35 ± 0.23	147.31 ± 0.24
$\Delta\chi^2_{\text{min}}$	-0.0089	0.95	-0.75	-4.5

these reductions are mainly due to increased uncertainties of the H_0 constraints due to the three extra parameters of the DMS20 model. Nevertheless, it is worth noting that SPT+WMAP+DESI reduce the discrepancy with SH0ES to roughly 1σ , due to both a genuine shift of the mean H_0

value toward higher values and the increased uncertainties. Although, this improvement is not present for the full prior results and it disappears also for the post-filtered results when PP is included in the data set.

Top panels of Fig. 4 illustrate the evolution of

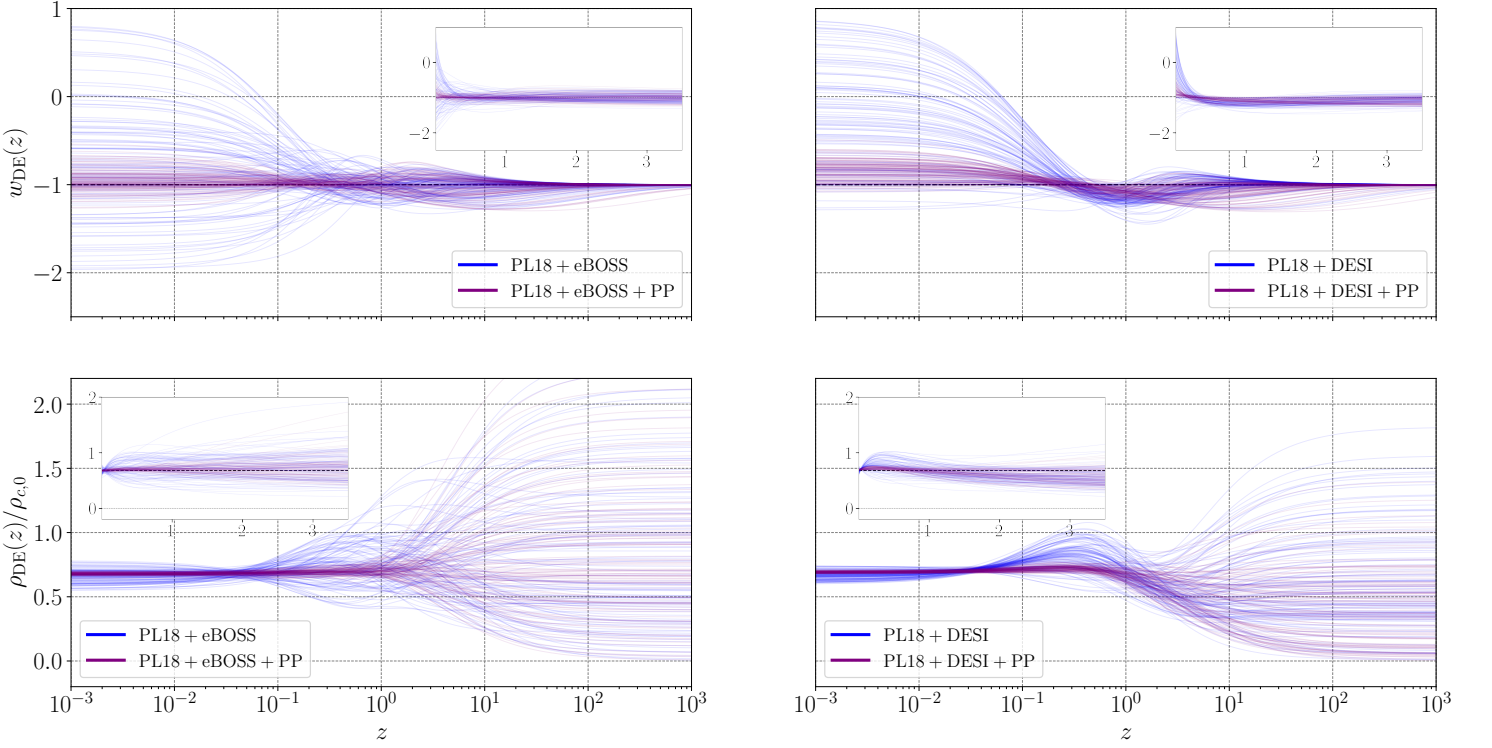


FIG. 8. Same as Fig. 7 but for the full-prior results.

TABLE V. 68% CL constraints on the free parameters (above the line) and derived parameters (below the line), obtained from the full-prior results using PL18 as the baseline CMB dataset.

	PL18+eBOSS	PL18+eBOSS+PP	PL18+DESI	PL18+DESI+PP
$\Omega_b h^2$	0.02238 ± 0.00014	0.02236 ± 0.00015	0.02245 ± 0.00014	0.02246 ± 0.00014
$\Omega_c h^2$	0.1200 ± 0.0011	0.1201 ± 0.0011	0.11904 ± 0.00098	0.11889 ± 0.00097
$100\theta_{MC}$	1.04092 ± 0.00030	1.04090 ± 0.00031	1.04105 ± 0.00029	1.04107 ± 0.00029
τ	0.0543 ± 0.0075	0.0546 ± 0.0075	0.0560 ± 0.0075	0.0566 ± 0.0075
$\ln(10^{10} A_s)$	3.045 ± 0.015	3.045 ± 0.015	3.046 ± 0.015	3.047 ± 0.015
n_s	0.9653 ± 0.0040	0.9652 ± 0.0039	0.9677 ± 0.0038	0.9681 ± 0.0038
α	$1.1^{+2.3}_{-3.5}$	$0.2^{+1.0}_{-1.3}$	1.1 ± 3.9	$0.2^{+1.2}_{-1.9}$
β	-0.3 ± 3.8	$-0.7^{+2.3}_{-1.7}$	< -2.12	$-0.5^{+2.3}_{-1.0}$
a_m	$0.62^{+0.28}_{-0.37}$	$0.75^{+0.27}_{-0.22}$	< 0.743	< 0.824
Ω_m	0.332 ± 0.052	0.3218 ± 0.0090	0.329 ± 0.036	0.3093 ± 0.0067
H_0 [km/s/Mpc]	$66.3^{+3.3}_{-6.9}$	66.70 ± 0.85	$66.1^{+3.1}_{-4.2}$	67.77 ± 0.69
S_8	$0.836^{+0.025}_{-0.019}$	$0.835^{+0.011}_{-0.013}$	$0.831^{+0.018}_{-0.016}$	0.823 ± 0.010
r_d [Mpc]	147.09 ± 0.25	147.10 ± 0.26	147.27 ± 0.23	147.29 ± 0.23
$\Delta\chi^2_{min}$	-0.46	0.32	-7.5	-5.6

the Hubble parameter for PL18+DESI, PL18+DESI+PP, SPT+WMAP+DESI, and SPT+WMAP+DESI+PP data set combinations of the post-filtered results, while the bottom panels present the corresponding results for the full-prior case. All these scenarios, along with the baseline Λ CDM model, remain discrepant with DESI LRG measurement at redshift $z = 0.510$, however, this is decreased for the

full prior results. These figures also visualize the discussions of the previous paragraph, where the post-filtered results for PL18+DESI and SPT+WMAP+DESI can be seen to reduce the H_0 tension relative to Λ CDM albeit with large uncertainties. As shown in the figures, the inclusion of PP data, reduces the uncertainty of H_0 around a low H_0 value in strong tension with the SH0ES measure-

ment. Comparing the top panels with the bottom ones, it is evident that post-filtering the model (or equivalently restricting its priors) to satisfy $\alpha > 0$ and $\beta > 0$ significantly alters its potential expansion history. However, these alterations become much less irrelevant when PP is also included in the data set.

Next, we present the evolution of the dark energy density, $\rho_{\text{DE}}(z)$, and the corresponding EoS parameter, $w_{\text{DE}}(z)$, derived from the posterior chains of our analysis, as shown in Figs. 5 and 7 for the post-filtered results, and in Figs. 6 and 8 for the full-prior ones. While noticeable deviations from a cosmological constant ($w = -1$) are permitted across all results, such behavior is not necessarily favored, as discussed previously. A further striking feature shared by all results is the generic occurrence of a double PDL crossing, characterized by opposite crossing directions in each instance. However, the full prior and post-filtered results differ noticeably, as the order of the PDL crossings may be reversed between them. Specifically, the post-filtered results show an initial crossing into the quintessence regime, followed by a second crossing into the phantom regime. This ordering is by construction, as the post-filtered results assume the existence of a PDL crossing from the quintessence to the phantom regime, which must be the latest crossing if multiple occur. In contrast, the full prior results may instead exhibit an initial crossing into the phantom regime, followed by a second one into the quintessence regime—although they can also display the same crossing pattern as the post-filtered results. However, note that, while the double PDL crossing is generic, it is not present in all the MCMC samples for either full or post-filtered results. A double crossing for the post-filtered results would correspond to a initially increasing DE density that goes through a decreasing phase before falling back to a decreasing regime; while this behavior describes the majority of the samples in Figs. 5 and 7, DE density evolutions that start with an initially increasing phase are also ubiquitous, especially when DESI is not present in the data set. Similar observations can be made for the full prior results. As a corollary to these discussions, we see that the present day value of the EoS parameter is always in the phantom regime for the post-filtered results by construction, but it is mostly in the quintessence regime for the full prior results especially when DESI is present in the data set combination. Addition of PP further clench this behavior. This late time preference of an quintessence EoS parameter from combinations of CMB DESI and PP data are in parallel with findings of [85, 88]. To quantify this preference (it also serves as a measure to quantify deviance from Λ CDM), we report constraints on the present-day dark energy equation of state parameter w_0 in Table VI for the full-prior results. The inferred values range from $w_0 = -0.93 \pm 0.13$ for the SPT+WMAP+eBOSS+PP combination to $w_0 = -0.34^{+0.53}_{-0.73}$ for PL18+DESI, indicating, depending on the specific case, a mild preference for quintessence-like behavior within the 2σ range. Although $w_0 = -1$ remains consistent with all datasets at the 95%

CL, the central values point to slight deviations from a pure cosmological constant, in agreement with the evolving trends in $\rho_{\text{DE}}(z)$ and $w_{\text{DE}}(z)$ discussed earlier.

TABLE VI. Values of w_0 for different dataset combinations (full-prior results). Uncertainties correspond to 68% CL, with 95% CL shown in parentheses.

Dataset	w_0
PL18+eBOSS	$-0.77^{+0.50}_{-0.85}$ (+1.5) (-1.2)
PL18+eBOSS+PP	$-0.93^{+0.11}_{-0.12}$ (+0.27) (-0.23)
PL18+DESI	$-0.34^{+0.53}_{-0.73}$ (+1.2) (-1.0)
PL18+DESI+PP	$-0.848^{+0.097}_{-0.16}$ (+0.27) (-0.22)
SPT+WMAP+eBOSS	$-0.85^{+0.52}_{-0.58}$ (+1.4) (-1.1)
SPT+WMAP+eBOSS+PP	$-0.93 \pm 0.13^{(+0.28)}$ (-0.25)
SPT+WMAP+DESI	$-0.44^{+0.58}_{-0.75}$ (+1.3) (-1.0)
SPT+WMAP+DESI+PP	$-0.86^{+0.11}_{-0.15}$ (+0.27) (-0.22)

V. CONCLUSION

In this work, we have carried out a comprehensive analysis of a dynamical dark energy model parameterized by $\{\alpha, \beta, a_m\}$, extending the prior ranges beyond those considered in previous studies to enable a broader exploration of the parameter space of the model. This extended framework allows for qualitatively richer evolution histories of the dark energy density $\rho_{\text{DE}}(z)$ and equation of state $w_{\text{DE}}(z)$, including possible phantom divide line (PDL) crossings in both directions. By combining a variety of observational datasets—including CMB measurements from SPT, WMAP, and Planck18; BAO data from eBOSS and DESI; and supernovae observations from Pantheon+ (PP)—we find mild indication for deviation from a cosmological constant at intermediate redshifts as our results are generally consistent with Λ CDM within 2σ or less. In particular, the EoS generically exhibit two PDL crossings in opposite directions in a single expansion history. These features are robust across different dataset combinations, suggesting that dynamical dark energy with physically nontrivial features might be present in a concordance model.

We also investigated the impact of prior choices by comparing results obtained from full-prior and post-filtered results. The post-filtered results assume the presence of a PDL crossing from quintessence to phantom regime, and are better comparable to Refs. [157, 158] that analyze the same DE model. The full priors reveal multimodal behavior highlighting the critical role of prior selection in capturing the full phenomenology of the model, as in this case, the preferred present-day value of the EoS parameter is in the quintessence regime unlike the post-filtered results that assume a present-day phantom value. They are both statistically consistent with -1 . For some data set combinations the H_0 tension is

ameliorated formally due to significantly enlarged uncertainties in comparison to the Λ CDM model, however the combination of our CMB, BAO and supernovae data give tight constraints on H_0 in strong tension with the SH0ES measurements.

A dynamical feature that consistently emerges across all combinations of our dataset is the presence of multiple crossings of the phantom divide line, $w_{\text{DE}} = -1$, within a single dark energy evolution history. If confirmed, this behavior would carry significant theoretical implications, as it is incompatible with the most mainstream extensions of the Λ CDM model. A single crossing of the PDL, while maintaining a strictly positive dark energy density, is incompatible with single scalar field models governed by a canonical Lagrangian [156], regardless of the sign of the kinetic term—thereby excluding both simple quintessence and phantom field scenarios as viable descriptions. Multiple crossings, especially those occurring in both directions, further tighten theoretical constraints, pointing to the necessity of more complex frameworks, such as *quintom* models or effective multi-fluid scenarios. While certain single-field phantom setups can accommodate transitions from $\rho_{\text{DE}} < 0$ with $w_{\text{DE}} > -1$ to $\rho_{\text{DE}} > 0$ with $w_{\text{DE}} < -1$ at late times [156], the richer phenomenology suggested by our constraints—including oscillatory behavior and sign changes in ρ_{DE} —cannot be captured within single scalar field theories. These findings motivate further investigation into fundamental realizations of ODE-like dynamics, including non-canonical

fields, coupled systems, or emergent dark sector phenomena that extend beyond the conventional scalar field paradigm.

VI. ACKNOWLEDGMENTS

SAA acknowledges the support of the DGAPA postdoctoral fellowship program at ICF-UNAM, Mexico. EDV is supported by a Royal Society Dorothy Hodgkin Research Fellowship. RCN thanks the financial support from the Conselho Nacional de Desenvolvimento Científico e Tecnológico (CNPq, National Council for Scientific and Technological Development) under the project No. 304306/2022-3, and the Fundação de Amparo à Pesquisa do Estado do RS (FAPERGS, Research Support Foundation of the State of RS) for partial financial support under the project No. 23/2551-0000848-3. Ö.A. acknowledges the support by the Turkish Academy of Sciences in the scheme of the Outstanding Young Scientist Award (TÜBA-GEBİP). AAS acknowledges the funding from ANRF, Govt. of India, under the research grant no. CRG/2023/003984. This article is based upon work from COST Action CA21136 Addressing observational tensions in cosmology with systematics and fundamental physics (CosmoVerse) supported by COST (European Cooperation in Science and Technology). The authors acknowledge the use of High-Performance Computing resources from the IT Services at the University of Sheffield.

-
- [1] L. Perivolaropoulos and F. Skara, Challenges for Λ CDM: An update, *New Astron. Rev.* **95**, 101659 (2022), 2105.05208.
 - [2] E. Abdalla *et al.*, Cosmology intertwined: A review of the particle physics, astrophysics, and cosmology associated with the cosmological tensions and anomalies, *JHEAp* **34**, 49 (2022), 2203.06142.
 - [3] E. Di Valentino, Challenges of the Standard Cosmological Model, *Universe* **8**, 399 (2022).
 - [4] P. J. E. Peebles (2024) 2405.18307.
 - [5] E. Di Valentino *et al.*, The CosmoVerse White Paper: Addressing observational tensions in cosmology with systematics and fundamental physics (2025), 2504.01669.
 - [6] E. Di Valentino *et al.*, Snowmass2021 - Letter of interest cosmology intertwined I: Perspectives for the next decade, *Astropart. Phys.* **131**, 102606 (2021), 2008.11283.
 - [7] E. Di Valentino *et al.*, Cosmology Intertwined III: $f\sigma_8$ and S_8 , *Astropart. Phys.* **131**, 102604 (2021), 2008.11285.
 - [8] E. Di Valentino *et al.*, Snowmass2021 - Letter of interest cosmology intertwined IV: The age of the universe and its curvature, *Astropart. Phys.* **131**, 102607 (2021), 2008.11286.
 - [9] E. Di Valentino *et al.*, Snowmass2021 - Letter of interest cosmology intertwined II: The hubble constant tension, *Astropart. Phys.* **131**, 102605 (2021), 2008.11284.
 - [10] O. Akarsu, E. O. Colgáin, A. A. Sen, and M. M. Sheikh-Jabbari, Λ CDM Tensions: Localising Missing Physics through Consistency Checks, *Universe* **10**, 305 (2024), 2402.04767.
 - [11] L. Verde, T. Treu, and A. G. Riess, Tensions between the Early and the Late Universe, *Nature Astron.* **3**, 891 (2019), 1907.10625.
 - [12] E. Di Valentino, O. Mena, S. Pan, L. Visinelli, W. Yang, A. Melchiorri, D. F. Mota, A. G. Riess, and J. Silk, In the realm of the Hubble tension—a review of solutions, *Class. Quant. Grav.* **38**, 153001 (2021), 2103.01183.
 - [13] P. Shah, P. Lemos, and O. Lahav, A buyer’s guide to the Hubble constant, *Astron. Astrophys. Rev.* **29**, 9 (2021), 2109.01161.
 - [14] M. Kamionkowski and A. G. Riess, The Hubble Tension and Early Dark Energy (2022), 2211.04492.
 - [15] L. Verde, N. Schöneberg, and H. Gil-Marín, A tale of many H_0 (2023), 2311.13305.
 - [16] E. Di Valentino and D. Brout, eds., *The Hubble Constant Tension*, Springer Series in Astrophysics and Cosmology (Springer, 2024).
 - [17] L. Perivolaropoulos, Hubble Tension or Distance Ladder Crisis? (2024), 2408.11031.

- [18] N. Aghanim *et al.* (Planck), Planck 2018 results. VI. Cosmological parameters, *Astron. Astrophys.* **641**, A6 (2020), [Erratum: *Astron. Astrophys.* 652, C4 (2021)], 1807.06209.
- [19] L. Balkenhol *et al.* (SPT-3G), Measurement of the CMB temperature power spectrum and constraints on cosmology from the SPT-3G 2018 TT, TE, and EE dataset, *Phys. Rev. D* **108**, 023510 (2023), 2212.05642.
- [20] T. Louis *et al.* (ACT), The Atacama Cosmology Telescope: DR6 Power Spectra, Likelihoods and Λ CDM Parameters (2025), 2503.14452.
- [21] W. L. Freedman, B. F. Madore, T. Hoyt, I. S. Jang, R. Beaton, M. G. Lee, A. Monson, J. Neeley, and J. Rich, Calibration of the Tip of the Red Giant Branch (TRGB), *Astrophys. J.* **891**, 57 (2020), 2002.01550.
- [22] S. Birrer *et al.*, TDCOSMO - IV. Hierarchical time-delay cosmography – joint inference of the Hubble constant and galaxy density profiles, *Astron. Astrophys.* **643**, A165 (2020), 2007.02941.
- [23] Q. Wu, G.-Q. Zhang, and F.-Y. Wang, An 8 percent determination of the Hubble constant from localized fast radio bursts, *Mon. Not. Roy. Astron. Soc.* **515**, L1 (2022), [Erratum: *Mon. Not. Roy. Astron. Soc.* 531, L8 (2024)], 2108.00581.
- [24] R. I. Anderson, N. W. Koblishke, and L. Eyer, Reconciling astronomical distance scales with variable red giant stars (2023), 2303.04790.
- [25] D. Scolnic, A. G. Riess, J. Wu, S. Li, G. S. Anand, R. Beaton, S. Casertano, R. Anderson, S. Dhawan, and X. Ke, CATS: The Hubble Constant from Standardized TRGB and Type Ia Supernova Measurements (2023), 2304.06693.
- [26] D. O. Jones *et al.*, Cosmological Results from the RAISIN Survey: Using Type Ia Supernovae in the Near Infrared as a Novel Path to Measure the Dark Energy Equation of State, *Astrophys. J.* **933**, 172 (2022), 2201.07801.
- [27] G. S. Anand, R. B. Tully, L. Rizzi, A. G. Riess, and W. Yuan, Comparing Tip of the Red Giant Branch Distance Scales: An Independent Reduction of the Carnegie-Chicago Hubble Program and the Value of the Hubble Constant, *Astrophys. J.* **932**, 15 (2022), 2108.00007.
- [28] W. L. Freedman, Measurements of the Hubble Constant: Tensions in Perspective, *Astrophys. J.* **919**, 16 (2021), 2106.15656.
- [29] S. A. Uddin *et al.*, Carnegie Supernova Project I and II: Measurements of H_0 Using Cepheid, Tip of the Red Giant Branch, and Surface Brightness Fluctuation Distance Calibration to Type Ia Supernovae*, *Astrophys. J.* **970**, 72 (2024), 2308.01875.
- [30] C. D. Huang *et al.*, The Mira Distance to M101 and a 4% Measurement of H_0 , *Astrophys. J.* **963**, 83 (2024), 2312.08423.
- [31] D. W. Pesce *et al.*, The Megamaser Cosmology Project. XIII. Combined Hubble constant constraints, *Astrophys. J. Lett.* **891**, L1 (2020), 2001.09213.
- [32] E. Kourkchi, R. B. Tully, G. S. Anand, H. M. Courtois, A. Dupuy, J. D. Neill, L. Rizzi, and M. Seibert, Cosmicflows-4: The Calibration of Optical and Infrared Tully–Fisher Relations, *Astrophys. J.* **896**, 3 (2020), 2004.14499.
- [33] J. Schombert, S. McGaugh, and F. Lelli, Using the Baryonic Tully–Fisher Relation to Measure H_0 , *Astron. J.* **160**, 71 (2020), 2006.08615.
- [34] J. P. Blakeslee, J. B. Jensen, C.-P. Ma, P. A. Milne, and J. E. Greene, The Hubble Constant from Infrared Surface Brightness Fluctuation Distances, *Astrophys. J.* **911**, 65 (2021), 2101.02221.
- [35] T. de Jaeger, L. Galbany, A. G. Riess, B. E. Stahl, B. J. Shappee, A. V. Filippenko, and W. Zheng, A 5 percent measurement of the Hubble–Lemaître constant from Type II supernovae, *Mon. Not. Roy. Astron. Soc.* **514**, 4620 (2022), 2203.08974.
- [36] Y. S. Murakami, A. G. Riess, B. E. Stahl, W. D. Kenworthy, D.-M. A. Pluck, A. Macoreta, D. Brout, D. O. Jones, D. M. Scolnic, and A. V. Filippenko, Leveraging SN Ia spectroscopic similarity to improve the measurement of H_0 (2023), 2306.00070.
- [37] L. Breuval, A. G. Riess, S. Casertano, W. Yuan, L. M. Macri, M. Romaniello, Y. S. Murakami, D. Scolnic, G. S. Anand, and I. Soszyński, Small Magellanic Cloud Cepheids Observed with the Hubble Space Telescope Provide a New Anchor for the SH0ES Distance Ladder, *Astrophys. J.* **973**, 30 (2024), 2404.08038.
- [38] W. L. Freedman, B. F. Madore, I. S. Jang, T. J. Hoyt, A. J. Lee, and K. A. Owens, Status Report on the Chicago-Carnegie Hubble Program (CCHP): Three Independent Astrophysical Determinations of the Hubble Constant Using the James Webb Space Telescope (2024), 2408.06153.
- [39] A. G. Riess *et al.*, JWST Validates HST Distance Measurements: Selection of Supernova Subsample Explains Differences in JWST Estimates of Local H_0 (2024), 2408.11770.
- [40] C. Vogl *et al.*, No rungs attached: A distance-ladder free determination of the Hubble constant through type II supernova spectral modelling (2024), 2411.04968.
- [41] D. H. Gao, Q. Wu, J. P. Hu, S. X. Yi, X. Zhou, and F. Y. Wang, Measuring Hubble constant using localized and unlocalized fast radio bursts (2024), 2410.03994.
- [42] D. Scolnic *et al.*, The Hubble Tension in our own Backyard: DESI and the Nearness of the Coma Cluster (2024), 2409.14546.
- [43] K. Said *et al.*, DESI Peculiar Velocity Survey – Fundamental Plane (2024), 2408.13842.
- [44] P. Boubel, M. Colless, K. Said, and L. Staveley-Smith, An improved Tully–Fisher estimate of H_0 , *Mon. Not. Roy. Astron. Soc.* **533**, 1550 (2024), 2408.03660.
- [45] D. Scolnic, P. Boubel, J. Byrne, A. G. Riess, and G. S. Anand, Calibrating the Tully–Fisher Relation to Measure the Hubble Constant (2024), 2412.08449.
- [46] S. Li, A. G. Riess, D. Scolnic, S. Casertano, and G. S. Anand, JAGB 2.0: Improved Constraints on the J-region Asymptotic Giant Branch-based Hubble Constant from an Expanded Sample of JWST Observations (2025), 2502.05259.
- [47] J. B. Jensen, J. P. Blakeslee, M. Cantiello, M. Cowles, G. S. Anand, R. B. Tully, E. Kourkchi, and G. Raimondo, The TRGB-SBF Project. III. Refining the HST Surface Brightness Fluctuation Distance Scale Calibration with JWST (2025), 2502.15935.
- [48] A. G. Riess *et al.*, A Comprehensive Measurement of the Local Value of the Hubble Constant with 1 km s⁻¹ Mpc⁻¹ Uncertainty from the Hubble Space Telescope and the SH0ES Team, *Astrophys. J. Lett.* **934**, L7 (2022), 2112.04510.

- [49] G. Efstathiou, A Lockdown Perspective on the Hubble Tension (with comments from the SH0ES team) (2020), [2007.10716](#).
- [50] E. Mortsell, A. Goobar, J. Johansson, and S. Dhawan, Sensitivity of the Hubble Constant Determination to Cepheid Calibration, *Astrophys. J.* **933**, 212 (2022), [2105.11461](#).
- [51] E. Mortsell, A. Goobar, J. Johansson, and S. Dhawan, The Hubble Tension Revisited: Additional Local Distance Ladder Uncertainties, *Astrophys. J.* **935**, 58 (2022), [2106.09400](#).
- [52] A. Sharon, D. Kushnir, W. Yuan, L. Macri, and A. Riess, Reassessing the constraints from SH0ES extragalactic Cepheid amplitudes on systematic blending bias, *Mon. Not. Roy. Astron. Soc.* **528**, 6861 (2024), [2305.14435](#).
- [53] A. G. Riess, G. S. Anand, W. Yuan, S. Casertano, A. Dolphin, L. M. Macri, L. Breuval, D. Scolnic, M. Perrin, and R. I. Anderson, Crowded No More: The Accuracy of the Hubble Constant Tested with High-resolution Observations of Cepheids by JWST, *Astrophys. J. Lett.* **956**, L18 (2023), [2307.15806](#).
- [54] A. Bhardwaj *et al.*, High-resolution Spectroscopic Metallicities of Milky Way Cepheid Standards and Their Impact on the Leavitt Law and the Hubble Constant, *Astrophys. J. Lett.* **955**, L13 (2023), [2309.03263](#).
- [55] D. Brout and A. Riess, The Impact of Dust on Cepheid and Type Ia Supernova Distances (2023), [2311.08253](#).
- [56] A. M. Dwomoh, E. R. Peterson, D. Scolnic, C. Ashall, J. M. DerKacy, A. Do, J. Johansson, D. O. Jones, A. G. Riess, and B. J. Shappee, Evaluating the Consistency of Cosmological Distances Using Supernova Siblings in the Near-infrared, *Astrophys. J.* **965**, 90 (2024), [2311.06178](#).
- [57] A. G. Riess, G. S. Anand, W. Yuan, S. Casertano, A. Dolphin, L. M. Macri, L. Breuval, D. Scolnic, M. Perrin, and I. R. Anderson, JWST Observations Reject Unrecognized Crowding of Cepheid Photometry as an Explanation for the Hubble Tension at 8σ Confidence, *Astrophys. J. Lett.* **962**, L17 (2024), [2401.04773](#).
- [58] L. Knox and M. Millea, Hubble constant hunter's guide, *Phys. Rev. D* **101**, 043533 (2020), [1908.03663](#).
- [59] K. Jedamzik, L. Pogosian, and G.-B. Zhao, Why reducing the cosmic sound horizon alone can not fully resolve the Hubble tension, *Commun. in Phys.* **4**, 123 (2021), [2010.04158](#).
- [60] N. Schöneberg, G. Franco Abellán, A. Pérez Sánchez, S. J. Witte, V. Poulin, and J. Lesgourgues, The H0 Olympics: A fair ranking of proposed models, *Phys. Rept.* **984**, 1 (2022), [2107.10291](#).
- [61] A. R. Khalife, M. B. Zanjani, S. Galli, S. Günther, J. Lesgourgues, and K. Benabed, Review of Hubble tension solutions with new SH0ES and SPT-3G data, *JCAP* **04**, 059, [2312.09814](#).
- [62] W. Giarè, [CMB Anomalies and the Hubble Tension](#) (2023), [2305.16919](#).
- [63] J.-P. Hu and F.-Y. Wang, Hubble Tension: The Evidence of New Physics, *Universe* **9**, 94 (2023), [2302.05709](#).
- [64] R. C. Nunes and S. Vagnozzi, Arbitrating the S8 discrepancy with growth rate measurements from redshift-space distortions, *Mon. Not. Roy. Astron. Soc.* **505**, 5427 (2021), [2106.01208](#).
- [65] E. Di Valentino and S. Bridle, Exploring the Tension between Current Cosmic Microwave Background and Cosmic Shear Data, *Symmetry* **10**, 585 (2018).
- [66] S. A. Adil, O. Akarsu, M. Malekjani, E. O. Colgáin, S. Pourojaghi, A. A. Sen, and M. M. Sheikh-Jabbari, S8 increases with effective redshift in Λ CDM cosmology, *Mon. Not. Roy. Astron. Soc.* **528**, L20 (2023), [2303.06928](#).
- [67] O. Akarsu, E. O. Colgáin, A. A. Sen, and M. M. Sheikh-Jabbari, Further support for S_8 increasing with effective redshift (2024), [2410.23134](#).
- [68] A. Amon *et al.* (DES), Dark Energy Survey Year 3 results: Cosmology from cosmic shear and robustness to data calibration, *Phys. Rev. D* **105**, 023514 (2022), [2105.13543](#).
- [69] L. F. Secco *et al.* (DES), Dark Energy Survey Year 3 results: Cosmology from cosmic shear and robustness to modeling uncertainty, *Phys. Rev. D* **105**, 023515 (2022), [2105.13544](#).
- [70] M. Asgari *et al.* (KiDS), KiDS-1000 Cosmology: Cosmic shear constraints and comparison between two point statistics, *Astron. Astrophys.* **645**, A104 (2021), [2007.15633](#).
- [71] M. Asgari *et al.*, KiDS+VIKING-450 and DES-Y1 combined: Mitigating baryon feedback uncertainty with COSEBIs, *Astron. Astrophys.* **634**, A127 (2020), [1910.05336](#).
- [72] S. Joudaki *et al.*, KiDS+VIKING-450 and DES-Y1 combined: Cosmology with cosmic shear, *Astron. Astrophys.* **638**, L1 (2020), [1906.09262](#).
- [73] G. D'Amico, J. Gleyzes, N. Kokron, K. Markovic, L. Senatore, P. Zhang, F. Beutler, and H. Gil-Marín, The Cosmological Analysis of the SDSS/BOSS data from the Effective Field Theory of Large-Scale Structure, *JCAP* **05**, 005, [1909.05271](#).
- [74] T. M. C. Abbott *et al.* (Kilo-Degree Survey, DES), DES Y3 + KiDS-1000: Consistent cosmology combining cosmic shear surveys, *Open J. Astrophys.* **6**, 2305.17173 (2023), [2305.17173](#).
- [75] T. Tröster *et al.*, Cosmology from large-scale structure: Constraining Λ CDM with BOSS, *Astron. Astrophys.* **633**, L10 (2020), [1909.11006](#).
- [76] C. Heymans *et al.*, KiDS-1000 Cosmology: Multi-probe weak gravitational lensing and spectroscopic galaxy clustering constraints, *Astron. Astrophys.* **646**, A140 (2021), [2007.15632](#).
- [77] R. Dalal *et al.*, Hyper Suprime-Cam Year 3 Results: Cosmology from Cosmic Shear Power Spectra (2023), [2304.00701](#).
- [78] S. Chen *et al.*, Not all lensing is low: An analysis of DESI \times DES using the Lagrangian Effective Theory of LSS (2024), [2407.04795](#).
- [79] J. Kim *et al.* (ACT, DESI), The Atacama Cosmology Telescope DR6 and DESI: Structure formation over cosmic time with a measurement of the cross-correlation of CMB Lensing and Luminous Red Galaxies (2024), [2407.04606](#).
- [80] L. Faga *et al.* (DES), Dark Energy Survey Year 3 Results: Cosmology from galaxy clustering and galaxy-galaxy lensing in harmonic space (2024), [2406.12675](#).
- [81] J. Harnois-Deraps *et al.*, KiDS-1000 and DES-Y1 combined: Cosmology from peak count statistics (2024), [2405.10312](#).
- [82] A. Dvornik *et al.*, KiDS-1000: Combined halo-model cosmology constraints from galaxy abundance, galaxy clustering and galaxy-galaxy lensing, *Astron. Astro-*

- phys. **675**, A189 (2023), 2210.03110.
- [83] T. M. C. Abbott *et al.* (DES), Dark Energy Survey Year 3 results: Cosmological constraints from galaxy clustering and weak lensing, *Phys. Rev. D* **105**, 023520 (2022), 2105.13549.
- [84] A. H. Wright *et al.*, KiDS-Legacy: Cosmological constraints from cosmic shear with the complete Kilo-Degree Survey (2025), 2503.19441.
- [85] A. G. Adame *et al.* (DESI), DESI 2024 VI: cosmological constraints from the measurements of baryon acoustic oscillations, *JCAP* **02**, 021, 2404.03002.
- [86] R. Calderon *et al.* (DESI), DESI 2024: reconstructing dark energy using crossing statistics with DESI DR1 BAO data, *JCAP* **10**, 048, 2405.04216.
- [87] A. G. Adame *et al.* (DESI), DESI 2024 V: Full-Shape Galaxy Clustering from Galaxies and Quasars (2024), 2411.12021.
- [88] M. Abdul Karim *et al.* (DESI), DESI DR2 Results II: Measurements of Baryon Acoustic Oscillations and Cosmological Constraints (2025), 2503.14738.
- [89] K. Lodha *et al.* (DESI), Extended Dark Energy analysis using DESI DR2 BAO measurements (2025), 2503.14743.
- [90] T. M. C. Abbott *et al.* (DES), The Dark Energy Survey: Cosmology Results with ~ 1500 New High-redshift Type Ia Supernovae Using the Full 5 yr Data Set, *Astrophys. J. Lett.* **973**, L14 (2024), 2401.02929.
- [91] T. M. C. Abbott *et al.* (DES), Dark Energy Survey: implications for cosmological expansion models from the final DES Baryon Acoustic Oscillation and Supernova data (2025), 2503.06712.
- [92] M. Cortès and A. R. Liddle, Interpreting DESI's evidence for evolving dark energy, *JCAP* **12**, 007, 2404.08056.
- [93] D. Shlivko and P. J. Steinhardt, Assessing observational constraints on dark energy, *Phys. Lett. B* **855**, 138826 (2024), 2405.03933.
- [94] O. Luongo and M. Muccino, Model-independent cosmographic constraints from DESI 2024, *Astron. Astrophys.* **690**, A40 (2024), 2404.07070.
- [95] W. Yin, Cosmic clues: DESI, dark energy, and the cosmological constant problem, *JHEP* **05**, 327, 2404.06444.
- [96] I. D. Gialamas, G. Hütsi, K. Kannike, A. Racioppi, M. Raidal, M. Vasar, and H. Veermäe, Interpreting DESI 2024 BAO: late-time dynamical dark energy or a local effect? (2024), 2406.07533.
- [97] B. R. Dinda, A new diagnostic for the null test of dynamical dark energy in light of DESI 2024 and other BAO data, *JCAP* **09**, 062, 2405.06618.
- [98] M. Najafi, S. Pan, E. Di Valentino, and J. T. Firouzjaee, Dynamical dark energy confronted with multiple CMB missions, *Phys. Dark Univ.* **45**, 101539 (2024), 2407.14939.
- [99] H. Wang and Y.-S. Piao, Dark energy in light of recent DESI BAO and Hubble tension (2024), 2404.18579.
- [100] Y. Tada and T. Terada, Quintessential interpretation of the evolving dark energy in light of DESI observations, *Phys. Rev. D* **109**, L121305 (2024), 2404.05722.
- [101] Y. Carloni, O. Luongo, and M. Muccino, Does dark energy really revive using DESI 2024 data?, *Phys. Rev. D* **111**, 023512 (2025), 2404.12068.
- [102] C.-G. Park, J. de Cruz Pérez, and B. Ratra, Using non-DESI data to confirm and strengthen the DESI 2024 spatially flat w_0w_a CDM cosmological parametrization result, *Phys. Rev. D* **110**, 123533 (2024), 2405.00502.
- [103] K. Lodha *et al.* (DESI), DESI 2024: Constraints on physics-focused aspects of dark energy using DESI DR1 BAO data, *Phys. Rev. D* **111**, 023532 (2025), 2405.13588.
- [104] O. F. Ramadan, J. Sakstein, and D. Rubin, DESI constraints on exponential quintessence, *Phys. Rev. D* **110**, L041303 (2024), 2405.18747.
- [105] A. Notari, M. Redi, and A. Tesi, Consistent theories for the DESI dark energy fit, *JCAP* **11**, 025, 2406.08459.
- [106] L. Orchard and V. H. Cárdenas, Probing dark energy evolution post-DESI 2024, *Phys. Dark Univ.* **46**, 101678 (2024), 2407.05579.
- [107] A. Hernández-Almada, M. L. Mendoza-Martínez, M. A. García-Aspeitia, and V. Motta, Phenomenological emergent dark energy in the light of DESI Data Release 1, *Phys. Dark Univ.* **46**, 101668 (2024), 2407.09430.
- [108] S. Pourojaghi, M. Malekjani, and Z. Davari, Cosmological constraints on dark energy parametrizations after DESI 2024: Persistent deviation from standard Λ CDM cosmology (2024), 2407.09767.
- [109] W. Giarè, M. Najafi, S. Pan, E. Di Valentino, and J. T. Firouzjaee, Robust preference for Dynamical Dark Energy in DESI BAO and SN measurements, *JCAP* **10**, 035, 2407.16689.
- [110] J. a. Rebouças, D. H. F. de Souza, K. Zhong, V. Miranda, and R. Rosenfeld, Investigating late-time dark energy and massive neutrinos in light of DESI Y1 BAO, *JCAP* **02**, 024, 2408.14628.
- [111] W. Giarè, Dynamical Dark Energy Beyond Planck? Constraints from multiple CMB probes, DESI BAO and Type-Ia Supernovae (2024), 2409.17074.
- [112] C.-G. Park, J. de Cruz Pérez, and B. Ratra, Is the w_0w_a CDM cosmological parameterization evidence for dark energy dynamics partially caused by the excess smoothing of Planck CMB anisotropy data? (2024), 2410.13627.
- [113] N. Menci, A. A. Sen, and M. Castellano, The Excess of JWST Bright Galaxies: A Possible Origin in the Ground State of Dynamical Dark Energy in the Light of DESI 2024 Data, *Astrophys. J.* **976**, 227 (2024), 2410.22940.
- [114] T.-N. Li, Y.-H. Li, G.-H. Du, P.-J. Wu, L. Feng, J.-F. Zhang, and X. Zhang, Revisiting holographic dark energy after DESI 2024 (2024), 2411.08639.
- [115] J.-X. Li and S. Wang, A comprehensive numerical study on four categories of holographic dark energy models (2024), 2412.09064.
- [116] A. Notari, M. Redi, and A. Tesi, BAO vs. SN evidence for evolving dark energy (2024), 2411.11685.
- [117] Q. Gao, Z. Peng, S. Gao, and Y. Gong, On the Evidence of Dynamical Dark Energy, *Universe* **11**, 10 (2025), 2411.16046.
- [118] R. Fikri, E. ElKhateeb, E. S. Lashin, and W. El Hanafy, A preference for dynamical phantom dark energy using one-parameter model with Planck, DESI DR1 BAO and SN data (2024), 2411.19362.
- [119] J.-Q. Jiang, D. Pedrotti, S. S. da Costa, and S. Vagnozzi, Non-parametric late-time expansion history reconstruction and implications for the Hubble tension in light of DESI (2024), 2408.02365.
- [120] J. Zheng, D.-C. Qiang, and Z.-Q. You, Cosmological constraints on dark energy models using DESI BAO 2024 (2024), 2412.04830.

- [121] A. Gómez-Valent and J. Solà Peracaula, Composite dark energy and the cosmological tensions, *Phys. Lett. B* **864**, 139391 (2025), 2412.15124.
- [122] S. Roy Choudhury and T. Okumura, Updated Cosmological Constraints in Extended Parameter Space with Planck PR4, DESI Baryon Acoustic Oscillations, and Supernovae: Dynamical Dark Energy, Neutrino Masses, Lensing Anomaly, and the Hubble Tension, *Astrophys. J. Lett.* **976**, L11 (2024), 2409.13022.
- [123] A. Lewis and E. Chamberlain, Understanding acoustic scale observations: the one-sided fight against Λ (2024), 2412.13894.
- [124] W. J. Wolf, C. García-García, and P. G. Ferreira, Robustness of Dark Energy Phenomenology Across Different Parameterizations (2025), 2502.04929.
- [125] A. J. Shajib and J. A. Frieman, Evolving dark energy models: Current and forecast constraints (2025), 2502.06929.
- [126] W. Giarè, T. Mahassen, E. Di Valentino, and S. Pan, An overview of what current data can (and cannot yet) say about evolving dark energy, *Phys. Dark Univ.* **48**, 101906 (2025), 2502.10264.
- [127] E. Chaussidon *et al.*, Early time solution as an alternative to the late time evolving dark energy with DESI DR2 BAO (2025), 2503.24343.
- [128] D. A. Kessler, L. A. Escamilla, S. Pan, and E. Di Valentino, One-parameter dynamical dark energy: Hints for oscillations (2025), 2504.00776.
- [129] M. Chevallier and D. Polarski, Accelerating universes with scaling dark matter, *Int. J. Mod. Phys. D* **10**, 213 (2001), gr-qc/0009008.
- [130] E. V. Linder, Exploring the expansion history of the universe, *Phys. Rev. Lett.* **90**, 091301 (2003), astro-ph/0208512.
- [131] E. Ozulker, Is the dark energy equation of state parameter singular?, *Phys. Rev. D* **106**, 063509 (2022), 2203.04167.
- [132] K. Dutta, Ruchika, A. Roy, A. A. Sen, and M. M. Sheikh-Jabbari, Beyond Λ CDM with low and high redshift data: implications for dark energy, *Gen. Rel. Grav.* **52**, 15 (2020), 1808.06623.
- [133] L. Visinelli, S. Vagnozzi, and U. Danielsson, Revisiting a negative cosmological constant from low-redshift data, *Symmetry* **11**, 1035 (2019), 1907.07953.
- [134] M. Malekjani, R. M. Conville, E. O. Colgáin, S. Pourajghi, and M. M. Sheikh-Jabbari, On redshift evolution and negative dark energy density in Pantheon + Supernovae, *Eur. Phys. J. C* **84**, 317 (2024), 2301.12725.
- [135] J. A. Vázquez, D. Tamayo, G. Garcia-Arroyo, I. Gómez-Vargas, I. Quiros, and A. A. Sen, Coupled Multi Scalar Field Dark Energy (2023), 2305.11396.
- [136] S. A. Adil, U. Mukhopadhyay, A. A. Sen, and S. Vagnozzi, Dark energy in light of the early JWST observations: case for a negative cosmological constant?, *JCAP* **10**, 072, 2307.12763.
- [137] A. Gómez-Valent, A. Favale, M. Migliaccio, and A. A. Sen, Late-time phenomenology required to solve the H_0 tension in view of the cosmic ladders and the anisotropic and angular BAO datasets, *Phys. Rev. D* **109**, 023525 (2024), 2309.07795.
- [138] O. Akarsu, S. Kumar, E. Özülker, and J. A. Vazquez, Relaxing cosmological tensions with a sign switching cosmological constant, *Phys. Rev. D* **104**, 123512 (2021), 2108.09239.
- [139] O. Akarsu, S. Kumar, E. Özülker, J. A. Vazquez, and A. Yadav, Relaxing cosmological tensions with a sign switching cosmological constant: Improved results with Planck, BAO, and Pantheon data, *Phys. Rev. D* **108**, 023513 (2023), 2211.05742.
- [140] O. Akarsu, A. De Felice, E. Di Valentino, S. Kumar, R. C. Nunes, E. Ozulker, J. A. Vazquez, and A. Yadav, Λ_s CDM cosmology from a type-II minimally modified gravity, *arXiv e-prints*, arXiv:2402.07716 (2024), 2402.07716.
- [141] Ö. Akarsu, A. De Felice, E. Di Valentino, S. Kumar, R. C. Nunes, E. Özülker, J. A. Vazquez, and A. Yadav, Cosmological constraints on Λ_s CDM scenario in a type II minimally modified gravity, *Phys. Rev. D* **110**, 103527 (2024), 2406.07526.
- [142] O. Akarsu, J. D. Barrow, L. A. Escamilla, and J. A. Vazquez, Graduated dark energy: Observational hints of a spontaneous sign switch in the cosmological constant, *Phys. Rev. D* **101**, 063528 (2020), 1912.08751.
- [143] O. Akarsu, E. Di Valentino, S. Kumar, R. C. Nunes, J. A. Vazquez, and A. Yadav, Λ_s CDM model: A promising scenario for alleviation of cosmological tensions, *arXiv e-prints*, arXiv:2307.10899 (2023), 2307.10899.
- [144] A. Yadav, S. Kumar, C. Kibris, and O. Akarsu, Λ_s CDM cosmology: alleviating major cosmological tensions by predicting standard neutrino properties, *JCAP* **01**, 042, 2406.18496.
- [145] L. A. Anchordoqui, I. Antoniadis, and D. Lust, Anti-de Sitter \rightarrow de Sitter transition driven by Casimir forces and mitigating tensions in cosmological parameters, *Phys. Lett. B* **855**, 138775 (2024), 2312.12352.
- [146] N. Menci, S. A. Adil, U. Mukhopadhyay, A. A. Sen, and S. Vagnozzi, Negative cosmological constant in the dark energy sector: tests from JWST photometric and spectroscopic observations of high-redshift galaxies, *JCAP* **07**, 072, 2401.12659.
- [147] L. A. Anchordoqui, I. Antoniadis, D. Lust, N. T. Noble, and J. F. Soriano, From infinite to infinitesimal: Using the Universe as a dataset to probe Casimir corrections to the vacuum energy from fields inhabiting the dark dimension, *Phys. Dark Univ.* **46**, 101715 (2024), 2404.17334.
- [148] L. A. Anchordoqui, I. Antoniadis, D. Bielli, A. Chattrabhuti, and H. Isono, Thin-wall vacuum decay in the presence of a compact dimension meets the H_0 and S_8 tensions (2024), 2410.18649.
- [149] J. F. Soriano, S. Wohlberg, and L. A. Anchordoqui, New insights on a sign-switching Λ , *Phys. Dark Univ.* **48**, 101911 (2025), 2502.19239.
- [150] A. De Felice, S. Kumar, S. Mukohyama, and R. C. Nunes, Observational bounds on extended minimal theories of massive gravity: new limits on the graviton mass, *JCAP* **04**, 013, 2311.10530.
- [151] A. Gomez-Valent and J. Solà Peracaula, Phantom Matter: A Challenging Solution to the Cosmological Tensions, *Astrophys. J.* **975**, 64 (2024), 2404.18845.
- [152] L. A. Escamilla, E. Özülker, O. Akarsu, E. Di Valentino, and J. A. Vázquez, Do we need wavelets in the late Universe? (2024), 2408.12516.
- [153] L. A. Escamilla, O. Akarsu, E. Di Valentino, and J. A. Vazquez, Model-independent reconstruction of the interacting dark energy kernel: Binned and Gaussian pro-

- cess, *JCAP* **11**, 051, 2305.16290.
- [154] M. A. Sabogal, O. Akarsu, A. Bonilla, E. Di Valentino, and R. C. Nunes, Exploring new physics in the late Universe's expansion through non-parametric inference, *Eur. Phys. J. C* **84**, 703 (2024), 2407.04223.
- [155] O. Akarsu, B. Bulduk, A. De Felice, N. Katirci, and N. M. Uzun, Unexplored regions in teleparallel $f(T)$ gravity: Sign-changing dark energy density (2024), 2410.23068.
- [156] O. Akarsu, L. Perivolaropoulos, A. Tsikoundoura, A. E. Yükselci, and A. Zhuk, Dynamical dark energy with AdS-to-dS and dS-to-dS transitions: Implications for the H_0 tension (2025), 2502.14667.
- [157] S. A. Adil, O. Akarsu, E. Di Valentino, R. C. Nunes, E. Özüiker, A. A. Sen, and E. Specogna, Omnipotent dark energy: A phenomenological answer to the Hubble tension, *Phys. Rev. D* **109**, 023527 (2024), 2306.08046.
- [158] E. Di Valentino, A. Mukherjee, and A. A. Sen, Dark Energy with Phantom Crossing and the H_0 Tension, *Entropy* **23**, 404 (2021), 2005.12587.
- [159] A. Bonilla, S. Kumar, and R. C. Nunes, Measurements of H_0 and reconstruction of the dark energy properties from a model-independent joint analysis, *Eur. Phys. J. C* **81**, 127 (2021), 2011.07140.
- [160] V. Sahni, A. Shafieloo, and A. A. Starobinsky, Model independent evidence for dark energy evolution from Baryon Acoustic Oscillations, *Astrophys. J. Lett.* **793**, L40 (2014), 1406.2209.
- [161] E. Aubourg *et al.*, Cosmological implications of baryon acoustic oscillation measurements, *Phys. Rev. D* **92**, 123516 (2015), 1411.1074.
- [162] Y. Wang, L. Pogosian, G.-B. Zhao, and A. Zucca, Evolution of dark energy reconstructed from the latest observations, *Astrophys. J. Lett.* **869**, L8 (2018), 1807.03772.
- [163] V. Poulin, K. K. Boddy, S. Bird, and M. Kamionkowski, Implications of an extended dark energy cosmology with massive neutrinos for cosmological tensions, *Phys. Rev. D* **97**, 123504 (2018), 1803.02474.
- [164] L. A. Escamilla and J. A. Vazquez, Model selection applied to reconstructions of the Dark Energy, *Eur. Phys. J. C* **83**, 251 (2023), 2111.10457.
- [165] A. A. Sen, S. A. Adil, and S. Sen, Do cosmological observations allow a negative Λ ?, *Mon. Not. Roy. Astron. Soc.* **518**, 1098 (2022), 2112.10641.
- [166] R. Calderón, R. Gannouji, B. L'Huillier, and D. Polarski, Negative cosmological constant in the dark sector?, *Phys. Rev. D* **103**, 023526 (2021), 2008.10237.
- [167] O. Akarsu, J. D. Barrow, C. V. R. Board, N. M. Uzun, and J. A. Vazquez, Screening Λ in a new modified gravity model, *Eur. Phys. J. C* **79**, 846 (2019), 1903.11519.
- [168] G. Acquaviva, O. Akarsu, N. Katirci, and J. A. Vazquez, Simple-graduated dark energy and spatial curvature, *Phys. Rev. D* **104**, 023505 (2021), 2104.02623.
- [169] O. Akarsu, E. O. Colgain, E. Özüiker, S. Thakur, and L. Yin, Inevitable manifestation of wiggles in the expansion of the late Universe, *Phys. Rev. D* **107**, 123526 (2023), 2207.10609.
- [170] R. R. Caldwell, A Phantom menace?, *Phys. Lett. B* **545**, 23 (2002), astro-ph/9908168.
- [171] E. V. Linder, Interpreting Dark Energy Data Away from Λ , *arXiv e-prints*, arXiv:2410.10981 (2024), 2410.10981.
- [172] A. Lewis, A. Challinor, and A. Lasenby, Efficient computation of CMB anisotropies in closed FRW models, *Astrophys. J.* **538**, 473 (2000), astro-ph/9911177.
- [173] C. Howlett, A. Lewis, A. Hall, and A. Challinor, CMB power spectrum parameter degeneracies in the era of precision cosmology, *JCAP* **04**, 027, 1201.3654.
- [174] J. Torrado and A. Lewis, Cobaya: Code for Bayesian Analysis of hierarchical physical models, *JCAP* **05**, 057, 2005.05290.
- [175] A. Lewis and S. Bridle, Cosmological parameters from CMB and other data: A Monte Carlo approach, *Phys. Rev. D* **66**, 103511 (2002), astro-ph/0205436.
- [176] R. M. Neal, Taking bigger metropolis steps by dragging fast variables (2005), math/0502099.
- [177] A. Lewis, Efficient sampling of fast and slow cosmological parameters, *Phys. Rev. D* **87**, 103529 (2013), 1304.4473.
- [178] D. Dutcher *et al.* (SPT-3G), Measurements of the E-mode polarization and temperature-E-mode correlation of the CMB from SPT-3G 2018 data, *Phys. Rev. D* **104**, 022003 (2021), 2101.01684.
- [179] G. Hinshaw, D. Larson, E. Komatsu, D. N. Spergel, C. L. Bennett, J. Dunkley, M. R.olta, M. Halpern, R. S. Hill, N. Odegard, L. Page, K. M. Smith, J. L. Weiland, B. Gold, N. Jarosik, A. Kogut, M. Limon, S. S. Meyer, G. S. Tucker, E. Wollack, and E. L. Wright, Nine-year wilkinson microwave anisotropy probe (wmap) observations: Cosmological parameter results, *The Astrophysical Journal Supplement Series* **208**, 19 (2013).
- [180] D. Collaboration, A. G. Adame, *et al.*, *Desi 2024 iii: Baryon acoustic oscillations from galaxies and quasars* (2024), 2404.03000.
- [181] D. Collaboration, A. G. Adame, *et al.*, *Desi 2024 iv: Baryon acoustic oscillations from the lyman alpha forest* (2024), 2404.03001.
- [182] S. Alam *et al.* (eBOSS), Completed SDSS-IV extended Baryon Oscillation Spectroscopic Survey: Cosmological implications from two decades of spectroscopic surveys at the Apache Point Observatory, *Phys. Rev. D* **103**, 083533 (2021), 2007.08991.
- [183] D. Brout *et al.*, The Pantheon+ Analysis: Cosmological Constraints, *Astrophys. J.* **938**, 110 (2022), 2202.04077.
- [184] A. Lewis, GetDist: a Python package for analysing Monte Carlo samples (2019), 1910.13970.
- [185] W. Handley, fgivenx: Functional posterior plotter, *The Journal of Open Source Software* **3**, 10.21105/joss.00849 (2018).
- [186] S. Alam *et al.* (eBOSS), Completed SDSS-IV extended Baryon Oscillation Spectroscopic Survey: Cosmological implications from two decades of spectroscopic surveys at the Apache Point Observatory, *Phys. Rev. D* **103**, 083533 (2021), 2007.08991.